RESEARCH ARTICLE SUMMARY

VACCINES

A mucosal vaccine against *Chlamydia trachomatis* generates two waves of protective memory T cells

Georg Stary,†* Andrew Olive,† Aleksandar F. Radovic-Moreno,† David Gondek, David Alvarez, Pamela A. Basto, Mario Perro, Vladimir D. Vrbanac, Andrew M. Tager, Jinjun Shi, Jeremy A. Yethon, Omid C. Farokhzad, Robert Langer, Michael N. Starnbach, Ulrich H. von Andrian*

INTRODUCTION: Administering vaccines through nonmucosal routes often leads to poor protection against mucosal pathogens, presumably because such vaccines do not generate memory lymphocytes that migrate to mucosal surfaces. Although mucosal vaccination induces mucosa-tropic memory lymphocytes, few mucosal vaccines are used clinically; live vaccine vectors pose safety risks, whereas killed pathogens or molecular antigens are usually weak immunogens when applied to intact mucosa. Adjuvants can boost immunogenicity; however, most conventional mucosal adjuvants have unfavorable safety profiles. Moreover, the immune mechanisms of protection against many mucosal infections are poorly understood.

RATIONALE: One case in point is *Chlamydia trachomatis* (*Ct*), a sexually transmitted intracellular bacterium that infects >100 million people annually. Mucosal *Ct* infections can cause female infertility and ectopic pregnancies. *Ct* is also the leading cause of preventable blindness in developing countries and induces pneumonia in infants. No approved vaccines exist to date. Here, we describe a *Ct* vaccine composed of ultraviolet light–inactivated *Ct* (UV-*Ct*) conjugated to charge-switching synthetic adjuvant nanoparticles (cSAPs). After immunizing mice with live *Ct*, UV-*Ct*, or UV-*Ct*–cSAP conjugates, we characterized mucosal immune responses to uterine *Ct* rechallenge and dissected the underlying cellular mechanisms.

RESULTS: In previously uninfected mice, *Ct* infection induced protective immunity that depended on CD4 T cells producing the cytokine interferon-γ, whereas uterine exposure to UV-*Ct* generated tolerogenic *Ct*-specific regulatory T cells, resulting in exacerbated bacterial burden upon *Ct* rechallenge. In contrast, mucosal immunization with UV-*Ct*–cSAP elicited long-lived protection. This differential effect of UV-*Ct*–cSAP versus UV-*Ct* was because the former was presented by immunogenic $CD11b^{+}CD103^{-}$ dendritic cells (DCs), whereas the latter was presented by tolerogenic $CD11b^{-}CD103^{+}$ DCs. Intrauterine or intranasal vaccination, but not subcutaneous vaccination, induced genital protection in both conventional and humanized mice. Regardless of vaccination route, UV-*Ct*–cSAP always evoked a robust systemic memory T cell response. However, only mucosal vaccination induced a wave of effector T cells that seeded the uterine mucosa during the first week after vaccination and established resident memory T cells (T_{RM} cells). Without T_{RM} cells, mice were suboptimally protected, even when circulating memory cells were abundant. Optimal *Ct* clearance required both early uterine seeding by T_{RM} cells and infection-induced recruitment of a second wave of circulating memory cells.

CONCLUSIONS: Mucosal exposure to both live *Ct* and inactivated UV-*Ct* induces antigen-specific CD4 T cell responses. While immunogenic DCs present the former to promote immunity, the latter is instead targeted to tolerogenic DCs that exacerbate host susceptibility to *Ct* infection. By combining UV-*Ct* with cSAP nanocarriers, we have redirected noninfectious UV-*Ct* to immunogenic DCs and achieved long-lived protection. This protective vaccine effect depended on the synergistic action of two memory T cell subsets with distinct differentiation kinetics and migratory properties. The cSAP technology offers a platform for efficient mucosal immunization that may also be applicable to other mucosal pathogens. ■

ON OUR WEB SITE

Read the full article at http://dx.doi.org/10.1126/science.aaa8205

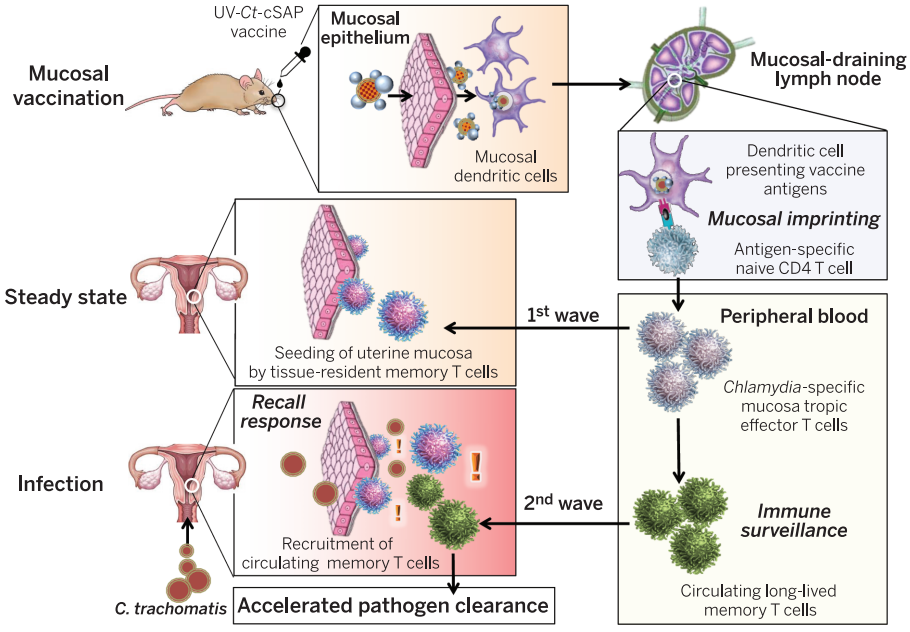

Protection against *C. trachomatis* infection after mucosal UV-*Ct*–cSAP vaccination. Upon mucosal vaccination, dendritic cells carry UV-*Ct*–cSAP to lymph nodes and stimulate CD4 T cells. Effector T cells are imprinted to traffic to uterine mucosa (first wave) and establish tissue-resident memory cells (T_{RM} cells). Vaccination also generates circulating memory T cells. Upon genital *Ct* infection, local reactivation of uterine T_{RM} cells triggers the recruitment of the circulating memory subset (second wave). Optimal pathogen clearance requires both waves of memory cells.

The list of affiliations is available in the full article online.
*Corresponding author. E-mail: uva@hms.harvard.edu (U.H.v.A.); georg_stary@hms.harvard.edu (G.S.) †These authors contributed equally to this work.
Cite this paper as G. Stary *et al.*, *Science* **348**, aaa8205 (2015). DOI: 10.1126/science.aaa8205

RESEARCH ARTICLE

VACCINES

A mucosal vaccine against *Chlamydia trachomatis* generates two waves of protective memory T cells

Georg Stary,[1]†* Andrew Olive,[1]† Aleksandar F. Radovic-Moreno,[2,3]† David Gondek,[1] David Alvarez,[1] Pamela A. Basto,[2,3] Mario Perro,[1] Vladimir D. Vrbanac,[4] Andrew M. Tager,[4] Jinjun Shi,[6] Jeremy A. Yethon,[5] Omid C. Farokhzad,[6,7] Robert Langer,[2,3] Michael N. Starnbach,[1] Ulrich H. von Andrian[1,8]*

Genital *Chlamydia trachomatis* (*Ct*) infection induces protective immunity that depends on interferon-γ–producing CD4 T cells. By contrast, we report that mucosal exposure to ultraviolet light (UV)–inactivated *Ct* (UV-*Ct*) generated regulatory T cells that exacerbated subsequent *Ct* infection. We show that mucosal immunization with UV-*Ct* complexed with charge-switching synthetic adjuvant particles (cSAPs) elicited long-lived protection in conventional and humanized mice. UV-*Ct*–cSAP targeted immunogenic uterine $CD11b^+CD103^-$ dendritic cells (DCs), whereas UV-*Ct* accumulated in tolerogenic $CD11b^-CD103^+$ DCs. Regardless of vaccination route, UV-*Ct*–cSAP induced systemic memory T cells, but only mucosal vaccination induced effector T cells that rapidly seeded uterine mucosa with resident memory T cells (T_{RM} cells). Optimal *Ct* clearance required both T_{RM} seeding and subsequent infection-induced recruitment of circulating memory T cells. Thus, UV-*Ct*–cSAP vaccination generated two synergistic memory T cell subsets with distinct migratory properties.

Although subcutaneous (s.c.) or intramuscular (i.m.) vaccination can generate efficient systemic and cutaneous immunity against many pathogens, vaccination by these nonmucosal routes often induces little or no protection at mucosal surfaces (*1*). A reason for this shortcoming is thought to be the differential imprinting of activated effector/memory lymphocytes in regional lymphoid tissues. These organs are populated by specialized antigen (Ag)–presenting dendritic cells (DCs) that induce the expression of tissue-specific homing receptors in T and B cells (*2*–*4*). Acquisition of tissue tropism enables the preferential migration of Ag-experienced lymphocytes to regions of the body that are associated with the secondary lymphoid organs where Ag was first encountered (*2*, *3*, *5*–*11*). Thus, whereas intracutaneous, s.c., and i.m. vaccines act in peripheral lymph nodes (LNs) to induce primarily skin-homing memory cells, mucosal vaccine exposure targets Ags into mucosa-associated lymphoid tissue (MALT) and focuses the ensuing memory response toward mucosal surfaces (*6*, *12*–*16*). However, only a handful of mucosal vaccines are currently available for use in humans, and most of these vaccines consist of replicating microorganisms, which may themselves cause infections in vulnerable individuals (*17*). Such safety concerns could be avoided with nonreplicating vaccines, such as killed pathogens or inanimate Ags; however, mucosal exposure to noninfectious Ags is typically insufficient to elicit a protective immune response unless the Ags are combined with potent adjuvants that are often too toxic for use in humans (*18*, *19*).

These immunobiological challenges present formidable obstacles to the development of effective vaccines for many mucosal pathogens. One prominent example among these "intractable" pathogens is *Chlamydia trachomatis* (*Ct*), a Gram-negative obligatory intracellular bacterium that infects mucosal epithelial cells. *Ct* is the most common sexually transmitted bacterial pathogen and is the leading cause of female infertility, ectopic pregnancy (*20*–*22*), and infectious blindness worldwide (*23*). Clinical trials in the 1960s with inactivated elementary bodies (EBs), the infectious form of *Ct* (*24*), achieved partial early protection, but at later stages some vaccinated individuals experienced more severe symptoms upon ocular *Ct* exposure than did placebo recipients (*24*–*30*). The underlying mechanism for this apparently enhanced risk of *Ct*-induced pathology after exposure to killed *Ct* is not understood. To this day, this persistent uncertainty has stymied further clinical development of *Ct* vaccines.

Effect of uterine mucosal exposure to live and killed *Ct*

Here, we used mice to explore the immunological consequences of mucosal exposure to live or killed *Ct* by performing intrauterine (i.u.) inoculations of either infectious *Ct* (serovar L2 unless stated otherwise) or ultraviolet light–inactivated *Ct* (UV-*Ct*). The animals were rechallenged with live *Ct* 4 weeks later, and uterine bacterial burden was assessed after 6 days (Fig. 1A). Consistent with earlier observations in this model (*31*), mice that had been previously infected with *Ct* acquired protective immunity, as evidenced by a factor of ~50 reduction in bacterial burden upon reinfection relative to naïve controls (Fig. 1B). In contrast, the bacterial burden in infected mice that had been previously exposed to UV-*Ct* was greater than in the nonimmunized group by a factor of 5 to 10. This exacerbated susceptibility to infection in the UV-*Ct* group was intriguingly reminiscent of the reported outcome of human vaccine trials five decades ago (*25*–*29*) and suggested that inactivated *Ct* was not merely "invisible" to the host immune system but somehow promoted tolerance.

Having thus determined that mucosal exposure to UV-*Ct* induces a pronounced tolerogenic immune response in mice, we asked whether mixing UV-*Ct* with an adjuvant could convert UV-*Ct* into an immunogen that might elicit protective immunity. However, i.u. injection of UV-*Ct* mixed with alum or with two different TLR agonists, imiquimod (TLR7 ligand) or CpG (TLR9 ligand), not only failed to confer protection but also rendered mice more susceptible to reinfection, similar to UV-*Ct* alone (Fig. 1C). Interestingly, when mice were instead immunized by s.c. injection, UV-*Ct* neither provoked a tolerogenic response nor conferred measurable protection, even when combined with adjuvants. Thus, the route of immunization can determine not only the tissue tropism of effector/memory cells but apparently also the tolerogenicity of a given Ag.

Conjugation of UV-inactivated *Ct* to charge-switching synthetic adjuvant particles

In light of these observations, we speculated that the lack of immunogenicity of i.u. exposure to crude mixtures of adjuvants with UV-*Ct* may have been due to differential permeability of the intact mucosal barrier to UV-*Ct* and/or free adjuvants. Thus, we reasoned that physical linkage of an adjuvant to UV-*Ct* may be necessary to allow both vaccine components to cross the epithelial barrier and be acquired by the same submucosal immunogenic DCs. To test this idea, we engineered modified charge-switching synthetic particles (cSPs), biodegradable nanocarriers that

[1]Division of Immunology, Department of Microbiology and Immunobiology, Harvard Medical School, Boston, MA 02115, USA. [2]Harvard-MIT Division of Health Sciences and Technology, Cambridge, MA 02139, USA. [3]Department of Chemical Engineering, Massachusetts Institute of Technology, Cambridge, MA 02139, USA. [4]Center for Immunology and Inflammatory Diseases, Massachusetts General Hospital, Harvard Medical School, Boston, MA 02114, USA. [5]Sanofi Pasteur, Cambridge, MA 02139, USA. [6]Laboratory of Nanomedicine and Biomaterials, Department of Anesthesiology, Brigham and Women's Hospital, Harvard Medical School, Boston, MA 02115, USA. [7]King Abdulaziz University, Jeddah, Saudi Arabia. [8]Ragon Institute of MGH, MIT and Harvard, Cambridge, MA 02139, USA.
*Corresponding author. E-mail: uva@hms.harvard.edu (U.H.v.A.); georg_stary@hms.harvard.edu (G.S.) †These authors contributed equally to this work.

were developed recently to target encapsulated antibiotics to bacterial surfaces (*32*). Using an emulsion-based manufacturing process, cSPs self-assemble from a triblock copolymer, poly (D,L-lactic-co-glycolic acid)-b-poly(L-histidine)-b-poly(ethylene glycol) (PLGA-PLH-PEG), to form a hydrophobic core (PLGA) and a hydrophilic surface consisting of PLH and PEG (*32*). At physiologic pH 7.4, cSPs carry a slight negative surface charge, but acidification to below pH 6.5 induces protonation of PLH imidazole groups, rendering cSPs cationic and allowing them to form conjugates with negatively charged bacteria (*32*). For use in vaccines, we modified cSPs by incorporating a second hydrophobic polymer, poly(D,L-lactic acid), that was covalently coupled to R848 (resiquimod), a potent TLR7/8 agonist (PLA-R848). Recent work has shown that after s.c. injection into mice, PEGylated PLA-R848–containing nanoparticles are phagocytosed by DCs and release free R848 within endosomes, resulting in efficient activation of endosomal TLR7 and DC maturation while minimizing systemic exposure to this adjuvant (*33*).

Thus, by incorporating R848 into cSPs, we created charge-switching synthetic adjuvant particles (cSAPs) that were then mixed with UV-*Ct* EBs in aqueous buffer (Fig. 1D). After acidification, cSAPs formed conjugates with UV-*Ct*, as confirmed by flow cytometry (Fig. 1, E and F), transmission electron microscopy (Fig. 1G), and dynamic light-scattering analysis (Fig. 1H). By contrast, synthetic adjuvant particles (SAPs) that lacked PLH and could not undergo surface-charge switching failed to bind UV-*Ct* and were used as a control.

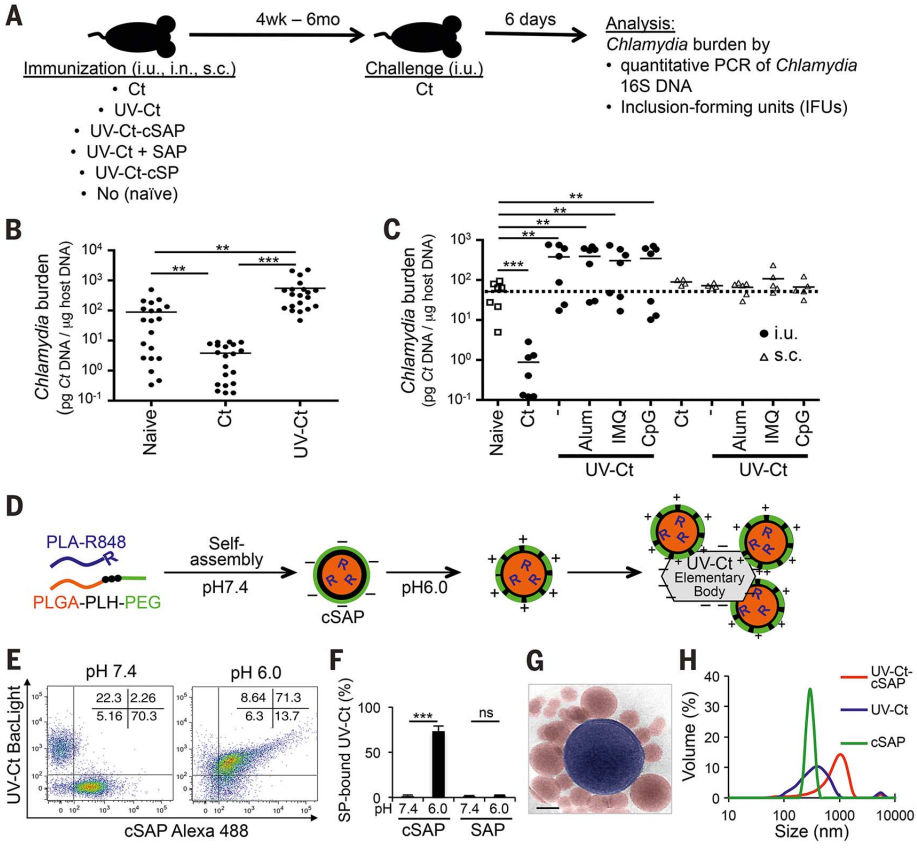

Fig. 1. Differential effects of immunization with *Ct*/UV-*Ct* and conjugation of UV-*Ct* with synthetic nanoparticles. (**A**) Schematic diagram of the immunization and challenge protocol for Fig. 1, B and C; Fig. 2, A, B, C, and F; Fig. 3, A and B; Fig. 4, E and F; Fig. 6A; and figs. S4 and S7. Mice were immunized with *Ct*, UV-*Ct*, UV-*Ct*–cSAP, or UV-*Ct* mixed with control nanoparticles (*Ct*, live *Chlamydia trachomatis*; UV-*Ct*, inactivated *Chlamydia trachomatis*; UV-*Ct*–cSAP, inactivated *Chlamydia trachomatis* complexed with charge-switching synthetic adjuvant particles; UV-*Ct* + SAP, inactivated *Chlamydia trachomatis* mixed with synthetic adjuvant particles (not attached to UV-Ct); UV-*Ct*–cSP–inactivated *Chlamydia trachomatis* complexed with charge-switching synthetic particles (without adjuvant)) via intrauterine (i.u.), intranasal (i.n.), or subcutaneous (s.c.) routes. Challenge with live *Ct* was always i.u. (**B**) Uterine *Ct* burden was measured by qPCR 6 days after i.u. challenge with live *Ct* in naïve mice and in animals that had been immunized 4 weeks earlier by i.u. injection of infectious *Ct* or UV-*Ct*. Data are pooled from 4 independent experiments (n = 20 mice per group; $^{**}P < 0.01$, $^{***}P < 0.001$; one-way ANOVA followed by Bonferroni posttest). (**C**) *Ct* burden after i.u. or s.c. immunization with UV-*Ct* mixed with adjuvants: alum, aluminum hydroxide; IMQ, imiquimod; CpG, CpG oligodeoxynucleotide type C (n = 5 to 7 mice per group; $^{**}P < 0.002$, $^{***}P < 0.001$; one-way ANOVA followed by Bonferroni posttest). (**D**) Schematic representation of surface charge-switching synthetic adjuvant particle (cSAP) production and conjugation to UV-*Ct*. (**E** and **F**) UV-*Ct* stained with BacLight was incubated with Alexa Fluor488–labeled cSAP or SAP at pH 7.4 or 6.0. (E) Representative FACS plots and (F) quantification of nanoparticle conjugates with UV-*Ct* from two independent experiments. $^{***}P < 0.001$; ns, not significant; two-tailed t tests. (**G**) A representative cryo–transmission electron micrograph of a UV-*Ct*–cSAP cluster showing cSAP in red and UV-Ct in blue. Scale bar, 100 nm. (**H**) Dynamic light scattering profiles of UV-*Ct*–cSAP, cSAP, and UV-*Ct* alone. The population distribution is representative of the volume scattering intensity. Data are representative of 10 independent experiments. Error bars represent mean ± SEM.

Effect of uterine mucosal vaccination with UV-*Ct*–cSAP conjugates

Having verified that cSAPs serve as an effective tool to attach a potent small-molecule adjuvant, R848, to UV-*Ct*, we compared the effect of i.u. exposure to UV-*Ct* alone or UV-*Ct* mixed with free SAPs (UV-*Ct* + SAP) or conjugated with either cSAPs (UV-*Ct*–cSAP) or adjuvant-free cSPs (UV-*Ct*–cSP), using the same i.u. prime/challenge protocol as above. Again, preconditioning with UV-*Ct* rendered mice hypersusceptible to subsequent *Ct* challenge, and this tolerogenic effect was preserved in animals that had received UV-*Ct* + SAP or UV-*Ct*–cSP (Fig. 2A). By contrast, bacterial clearance was accelerated in mice that had been immunized with UV-*Ct*–cSAP (Fig. 2B). Remarkably, the extent of vaccine-induced protection was equivalent, if not superior, relative to animals with "natural" memory after previous *Ct* infection. These results were independently confirmed when uteri of challenged mice were analyzed by blinded observers for the presence of infectious *Ct* by in vitro testing of tissue extracts for inclusion-forming units in McCoy cells (Fig. 2C and fig. S1). Robust protection was also achieved when cSAPs were conjugated to formalin-inactivated *Ct* (fig. S2A) or to another UV-inactivated strain of *Ct*, serotype E (*Ct-E*) (fig. S2B), or to *C. muridarum* (*Cm*), a mouse-adapted strain (Fig. 2D).

Although pathological changes in murine uteri infected with human-adapted strains of *Ct* are variable, infection of naïve mice with *Cm* caused reproducible tissue damage resulting in accumulation of serous exudate in fallopian tubes (hydrosalpinx), reminiscent of the pathology induced by chronic *Ct* infection in humans. By contrast, animals that had received i.u. UV-*Cm*–cSAP vaccination were profoundly protected against hydrosalpinx formation relative to naïve animals or recipients of UV-*Cm* alone (Fig. 2E).

The differential effects of i.u. conditioning with UV-*Ct*–cSAP and UV-*Ct* persisted unabated for at least 6 months; the former continued to afford profound protection, whereas the latter predisposed to enhanced susceptibility to *Ct* rechallenge. These findings indicate that mucosal exposure to UV-*Ct* in both immunogenic and tolerogenic contexts elicits sustained and qualitatively unchanging memory (Fig. 2F).

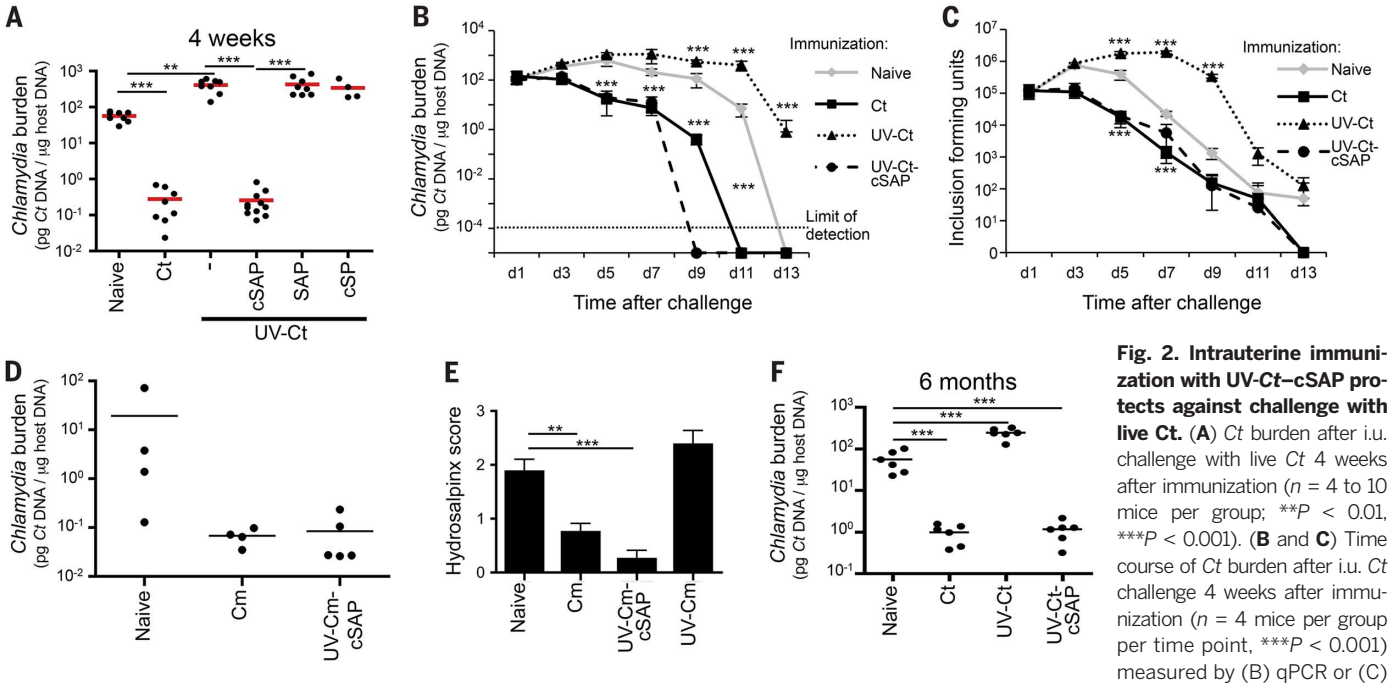

Fig. 2. Intrauterine immunization with UV-*Ct*–cSAP protects against challenge with live Ct. (**A**) *Ct* burden after i.u. challenge with live *Ct* 4 weeks after immunization (n = 4 to 10 mice per group; $^{**}P < 0.01$, $^{***}P < 0.001$). (**B** and **C**) Time course of *Ct* burden after i.u. *Ct* challenge 4 weeks after immunization (n = 4 mice per group per time point, $^{***}P < 0.001$) measured by (B) qPCR or (C) in vitro assessment of inclusion-forming units (IFUs). (**D**) *Ct* burden after intravaginal challenge with *Cm* 4 weeks after immunization with *Cm* and UV-*Cm*–cSAP. n = 3 or 4 mice per group; $^{***}P < 0.001$. (**E**) Gross uterine pathology determined as hydrosalpinx score 4 weeks after intravaginal challenge of immunized and naïve mice with *Cm* (n = 8 mice per group; $^{**}P < 0.01$, $^{***}P < 0.001$. (**F**) *Ct* burden after i.u. *Ct* challenge 6 months after i.u. immunization (n = 4 to 10 mice per group; $^{***}P < 0.001$). Statistical differences were assessed using one-way ANOVA followed by Bonferroni posttest.

UV-*Ct*–cSAP vaccination induces *Ct*-specific protective T helper 1 memory cells

Because the charge-based conjugation of cSAPs to UV-*Ct* was apparently sufficient not only to permanently avert the default tolerance response to UV-*Ct* but also to produce robust long-term protective immunity that prevented infection-induced tissue damage, we set out to dissect the underlying immunological mechanisms. Recent clinical evidence suggests that humans develop at least partially protective immunity upon clearance of genital *Ct* infection, whereby interferon (IFN)–γ production, presumably by T helper 1 (T_H1) cells, was inversely correlated with the risk for reinfection (*34*–*36*). Although mechanistic information in humans is sparse and far from definitive, the available data are consistent with experiments in mice where bacterial clearance after genital *Ct* or *Cm* infection is known to require T_H1 cells (*31*, *37*, *38*). Mouse experiments have also shown that during *Ct* or *Cm* infection, naïve T cells (T_N cells) differentiate into effector T cells (T_{Eff} cells) in uterus-draining lymph nodes (LNs), and these T_{Eff} cells are then recruited to the genital mucosa to mediate bacterial clearance (*39*–*41*). T_H1 cells are also a key component of long-term protective memory after infection, although a role for B cells and antibodies has also been reported (*42*–*47*).

Our analysis of UV-*Ct*–cSAP immunized mice revealed a robust *Ct*-specific antibody response that was equivalent to that elicited by *Ct* infection and about twice as great as in UV-*Ct*–exposed mice (fig. S3A). Moreover, i.u. immunization with UV-*Ct*–cSAP increased uterine mucosa-resident CD8 T cells (fig. S3B) as well as CD4 T cells (see below). To determine which component(s) of this multifaceted response to UV-*Ct*–cSAP were required for mucosal protection, we measured bacterial burdens after genital *Ct* infection in vaccinated mutant mice that lacked either B cells (μMt mice, which contain a deletion of the IgM heavy chain) or CD8 T cells (*Cd8*$^{-/-}$ mice) or CD4 T cells [B6.129S2-H2$^{dlAb1\text{-}Ea}$/J (referred to as MHC-II$^{-/-}$) mice (*48*)] or both B and T cells (*Rag2*$^{-/-}$ mice). Neither the absence of B cells nor that of CD8 T cells had a detectable impact on bacterial levels, whereas *Rag2*$^{-/-}$ mice (fig. S4) and MHC-II$^{-/-}$ mice were completely unprotected against *Ct* challenge (Fig. 3A). Of note, unlike wild-type animals, mice that were devoid of CD4 T cells did not suffer increased bacterial burdens after UV-*Ct* conditioning, indicating that CD4$^+$ T cells are needed not only for pathogen clearance but also for UV-*Ct*–induced tolerance.

Because the above experiments demonstrated that CD4 T cells are required for the sequelae of both UV-*Ct* and UV-*Ct*–cSAP exposure, we asked whether CD4 T cells alone were sufficient to confer these effects. Thus, we adoptively transferred purified leukocyte subsets from immunized mice to naïve recipients that were subsequently challenged with *Ct*. Partial protection against genital *Ct* challenge was achieved after transferring 10^7 splenic CD4 T cells from mice that had received i.u. injections of either *Ct* or UV-*Ct*–cSAP, whereas transfer of CD8 T cells or T cell–depleted splenocytes had no effect (Fig. 3B). Transfer of CD4 T cells from UV-*Ct*–conditioned donors conferred enhanced susceptibility to infection.

Having determined that CD4 memory T cells are both necessary and sufficient for *Ct*-specific protective memory, as well as tolerance, after immunization with UV-*Ct*–cSAP and UV-*Ct*, respectively, we asked how *Ct*-specific CD4 T_N cells respond to either stimulus, as compared to *Ct* infection. To this end, we adoptively transferred T_N cells from CD90.1$^+$ transgenic NR1 mice (*40*), in which most CD4 T cells express a *Ct*-specific T cell receptor (TCR) (fig. S5), into groups of congenic (CD90.2$^+$) hosts that were subsequently immunized i.u. with *Ct*, UV-*Ct*, or UV-*Ct*–cSAP. Four days later, NR1 cells had responded identically to *Ct* infection and UV-*Ct*–cSAP immunization; they had vigorously proliferated and expanded in the draining LNs (Fig. 3, C and D), and they also accumulated in the uterine mucosa (Fig. 3E). Moreover, upon in vitro rechallenge with UV-*Ct* pulsed autologous DCs, the vast majority of uterine and LN-resident NR1 cells in both groups produced one or more effector cytokines, including IFN-γ, interleukin (IL)–2, and tumor necrosis factor (TNF)–α (Fig. 3F). By contrast, in UV-*Ct*–exposed animals, NR1 cells showed less proliferation and accumulation in LNs and uterus, and they secreted little or no cytokines, similar to T_N cells.

Mucosal exposure to UV-*Ct* generates *Ct*-specific regulatory T cells

Although the encounter of UV-*Ct* evoked a blunted T_{Eff} response by *Ct*-specific CD4 T cells, this effect alone cannot explain why UV-*Ct* enhanced host

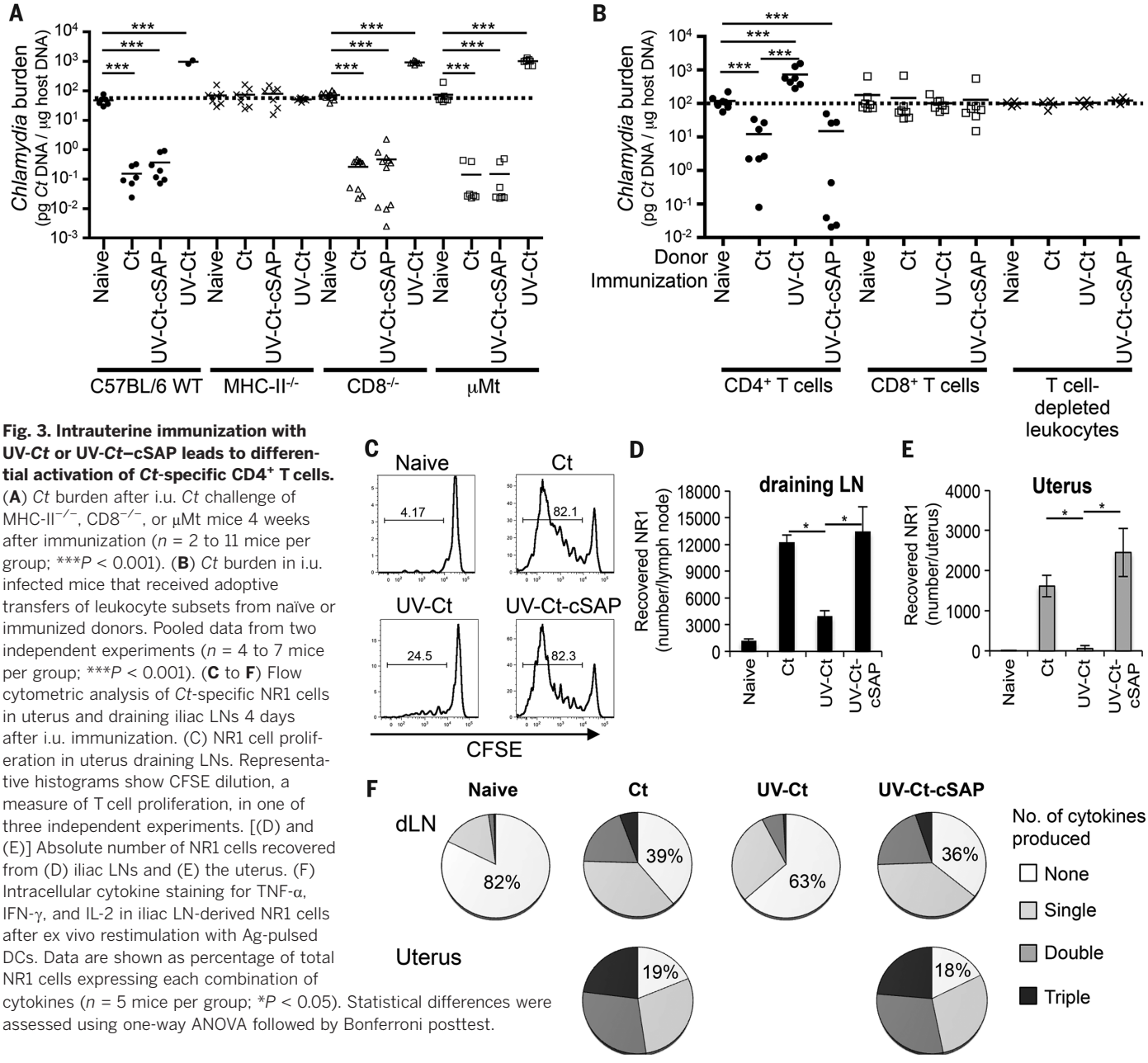

Fig. 3. Intrauterine immunization with UV-*Ct* or UV-*Ct*–cSAP leads to differential activation of *Ct*-specific CD4⁺ T cells. (**A**) *Ct* burden after i.u. *Ct* challenge of MHC-II$^{-/-}$, CD8$^{-/-}$, or µMt mice 4 weeks after immunization (n = 2 to 11 mice per group; ***P < 0.001). (**B**) *Ct* burden in i.u. infected mice that received adoptive transfers of leukocyte subsets from naïve or immunized donors. Pooled data from two independent experiments (n = 4 to 7 mice per group; ***P < 0.001). (**C** to **F**) Flow cytometric analysis of *Ct*-specific NR1 cells in uterus and draining iliac LNs 4 days after i.u. immunization. (C) NR1 cell proliferation in uterus draining LNs. Representative histograms show CFSE dilution, a measure of T cell proliferation, in one of three independent experiments. [(D) and (E)] Absolute number of NR1 cells recovered from (D) iliac LNs and (E) the uterus. (F) Intracellular cytokine staining for TNF-α, IFN-γ, and IL-2 in iliac LN-derived NR1 cells after ex vivo restimulation with Ag-pulsed DCs. Data are shown as percentage of total NR1 cells expressing each combination of cytokines (n = 5 mice per group; *P < 0.05). Statistical differences were assessed using one-way ANOVA followed by Bonferroni posttest.

susceptibility to subsequent *Ct* infection. The apparent tolerogenicity of UV-*Ct* clearly depended on CD4 T cells, because UV-*Ct* did not tolerize MHC-II$^{-/-}$ mice (Fig. 3A), whereas adoptive transfer of CD4 T cells from UV-*Ct*–conditioned wild-type mice conferred tolerance to naïve recipients (Fig. 3B). Thus, we hypothesized that mucosal UV-*Ct* exposure not only may compromise T_{Eff} differentiation of *Ct*-specific T_N cells but also may instigate an alternative "career decision" driving CD4 T_N cells to differentiate into FoxP3$^+$ CD25$^+$ regulatory T cells (T_{regs}). To test this idea, we adoptively transferred to naïve hosts T_N cells from NR1xFoxP3-eGFP donors after sorting the enhanced green fluorescent protein (eGFP)–negative fraction (i.e., non-T_{reg}). Recipients were then immunized with live *Ct*, UV-*Ct*, or UV-*Ct*–cSAP. Indeed, there was a massive increase in FoxP3-eGFP$^+$CD25$^+$ NR1 cells in the draining LNs (Fig. 4, A and B) and uterus (Fig. 4, C and D) of UV-*Ct*–exposed mice, whereas very few NR1 cells assumed a T_{reg} phenotype in response to *Ct* infection or UV-*Ct*–cSAP vaccination. Because a priori eGFP$^+$ T_{regs} had been removed before T_N transfer, the appearance of eGFP$^+$ T_{regs} after UV-*Ct* exposure was due to conversion of conventional T_N cells rather than to expansion of existing T_{regs}. These newly induced T_{regs} were required for tolerance to *Ct* infection, because anti-CD25–mediated T_{reg} depletion in UV-*Ct*–treated mice reduced uterine *Ct* burden upon subsequent infection to levels comparable to naïve mice (Fig. 4E). Moreover, UV-*Ct*–conditioned *Il10*$^{-/-}$ mice did not suffer enhanced bacterial burdens upon i.u. *Ct* challenge (Fig. 4F), which suggests that the de novo induced *Ct*-specific T_{regs} exerted their tolerogenic activity through the IL-10 pathway.

Differential mucosal antigen uptake and presentation by uterine dendritic cell subsets

What mechanisms are responsible for the differential T cell response to *Ct* or UV-*Ct*–cSAP versus UV-*Ct*? To address this question, we examined the phenotype and function of the three predominant uterus-resident MHC-II$^+$ leukocyte populations (fig. S6A): F4/80$^+$CD11b$^+$ macrophages that were CD11c$^{-/low}$, CD103$^-$, and expressed variable levels of CX3CR1, as well as two equally sized subsets of CD11c$^+$F4/80$^-$ DCs. One DC subset was CD103$^+$

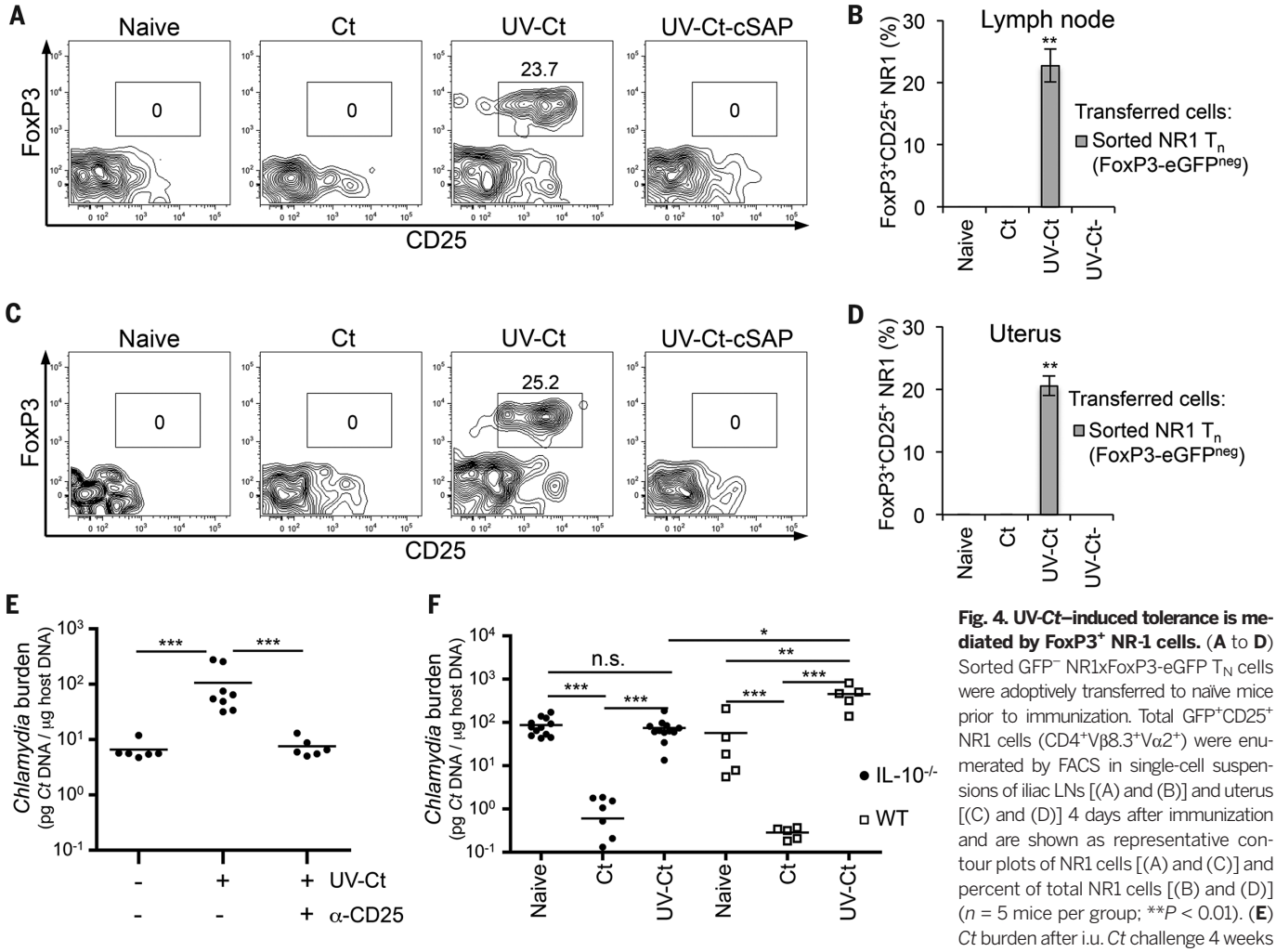

Fig. 4. UV-*Ct*–induced tolerance is mediated by FoxP3$^+$ NR-1 cells. (**A** to **D**) Sorted GFP$^-$ NR1xFoxP3-eGFP T_N cells were adoptively transferred to naïve mice prior to immunization. Total GFP$^+$CD25$^+$ NR1 cells (CD4$^+$Vβ8.3$^+$Vα2$^+$) were enumerated by FACS in single-cell suspensions of iliac LNs [(A) and (B)] and uterus [(C) and (D)] 4 days after immunization and are shown as representative contour plots of NR1 cells [(A) and (C)] and percent of total NR1 cells [(B) and (D)] (n = 5 mice per group; $^{**}P < 0.01$). (**E**) *Ct* burden after i.u. *Ct* challenge 4 weeks after immunization with *Ct*, UV-*Ct*, or UV-*Ct*–cSAP. In some animals T_{regs} were depleted with CD25 mAb (clone PC61) while the other groups received isotype-matched IgG 3 days before and after challenge (n = 6 mice per group; $^{***}P < 0.001$). (**F**) *Ct* burden after i.u. challenge with live *Ct* 4 weeks after immunization of *Il10*$^{-/-}$ mice (n = 5 to 11 mice per group; $^{*}P < 0.05$, $^{**}P < 0.01$, $^{***}P < 0.001$). Error bars depict mean ± SEM. Statistical differences were assessed using one-way ANOVA followed by Bonferroni posttest.

and expressed neither CD11b nor CX3CR1; the second DC population was CD103$^-$CD11b$^+$CX3CR1$^+$ (fig. S6B). All three populations were negative for CD207/Langerin and CD301b. Each of these candidate Ag-presenting cells (APCs) was sorted from single-cell suspensions of uteri or draining LNs of naïve and challenged mice and tested for *Ct* content and ability to stimulate NR1 T_N in vitro and in vivo (Fig. 5A). At 18 hours after i.u. exposure to *Ct*, UV-*Ct*, or UV-*Ct*–cSAP, uterine APCs had not changed significantly in total number or composition (fig. S6, C and D), and the amount of *Ct*-derived genetic material [determined by quantitative polymerase chain reaction (qPCR)] acquired by both macrophages and CD326$^+$ mucosal epithelial cells was similar in each group (Fig. 5B). By contrast, marked differences were apparent among the two DC subsets: live *Ct* and UV-*Ct*–cSAP were primarily acquired by CD103$^-$ DCs, whereas UV-*Ct* accumulated preferentially in CD103$^+$ DCs. Similarly, at 24 hours after challenge, when sorted APCs were isolated from uterus-draining LNs, bacterial loads were exclusively detected in CD103$^-$ DCs after genital exposure to *Ct* and UV-*Ct*–cSAP but not UV-*Ct* (Fig. 5C).

Consistent with the differential acquisition of *Ct*-derived genetic material, 3-day cocultures of purified uterine APC subsets with NR1 T_N cells revealed that CD103$^-$ DCs were singularly efficient at inducing T cell proliferation when they had been isolated from animals exposed to either *Ct* or UV-*Ct*–cSAP. By contrast, among UV-*Ct*–exposed APCs, only the CD103$^+$ DCs promoted substantial proliferation of NR1 T cells, whereas macrophages failed to induce T cell proliferation regardless of the immunization regimen (Fig. 5D). This differential APC activity was recapitulated when APC subsets were isolated from vaccinated animals and injected into footpads of naïve mice that had previously received NR1 T_N cells; CD103$^-$ DCs, but not CD103$^+$ DCs or macrophages, from *Ct*-infected and UV-*Ct*–cSAP–immunized mice stimulated NR1 T_N cell proliferation in the recipients' draining LNs (Fig. 5E). Footpad injection of sorted CD103$^+$ DCs did not promote a significant in vivo response by NR1 cells in this experimental setting; however, when CD103$^+$ DCs were isolated from UV-*Ct*–conditioned donors and exposed in vitro to NR1 T_N cells, they uniquely promoted the appearance of FoxP3$^+$CD25$^+$ T_{regs} (Fig. 5F).

In line with these functional observations, 18 hours after *Ct* infection or UV-*Ct*–cSAP immunization, uterine CD103$^-$ DCs preferentially up-regulated immunostimulatory molecules, including CD80, CD86, and IL-12 (Fig. 5G and fig. S6E). In contrast, upon immunization with UV-*Ct*, CD103$^+$ DCs selectively up-regulated certain anti-inflammatory pathways, including PD-L2 and IL-10. However, other markers of tolerogenic APCs either remained unchanged or were undetectable on uterine CD103$^+$ DCs, such as PD-L1 and RALDH, respectively.

We conclude that after mucosal exposure to live *Ct* and UV-*Ct*–cSAP, antigenic material is preferentially acquired and transported to the draining LNs by local immunostimulatory CD103$^-$ DCs, whereas exposure to UV-*Ct* results in Ag

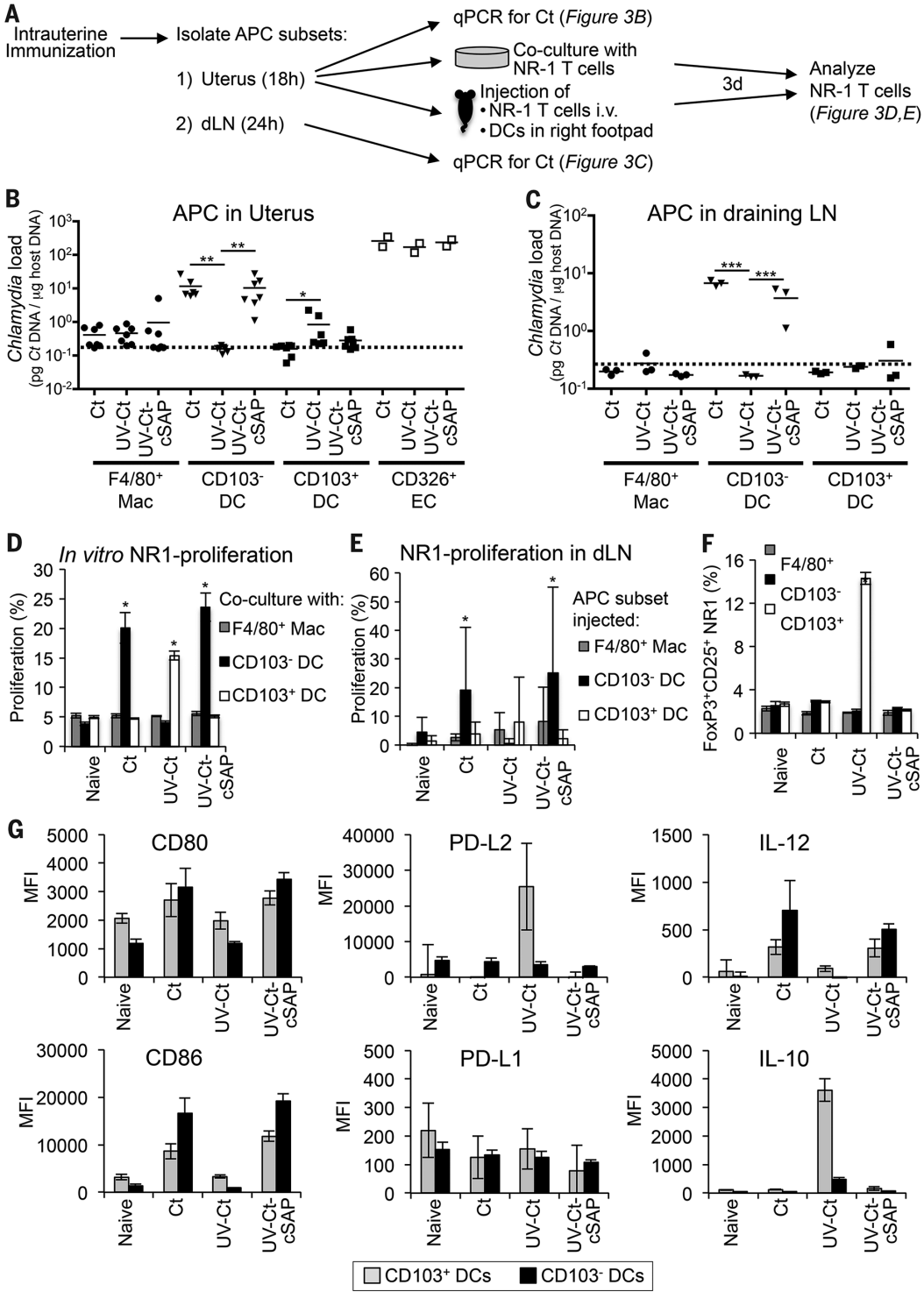

Fig. 5. Distinct uterine DC subsets acquire Ags after i.u. *Ct* and UV-*Ct*–cSAP versus UV-*Ct* immunization and induce differential responses by *Ct*-specific T cells in vitro and in vivo. (**A**) Schematic diagram of the experimental protocol for (B) to (F). Mice were immunized i.u. with *Ct*, UV-*Ct*, or UV-*Ct*–cSAP. At indicated time points thereafter, $CD45^+MHC\text{-}II^+$ APC subsets were isolated from uteri and LNs and FACS sorted according to CD103 and F4/80 expression. (**B** and **C**) Uptake of *Ct* per 1000 sorted APCs in the uterus (B) and draining LN (C) was measured by qPCR. Isolated uterine $CD326^+$ epithelial cells (EC) served as positive control for uterine samples. Data are pooled from two independent experiments. Mac, macrophages; DC, dendritic cells. $n = 2$ to 7; broken line, limit of detection; $^*P < 0.05$, $^{**}P < 0.01$, $^{***}P < 0.001$. (**D**) In vitro proliferation of NR1 T_N was determined by CFSE dilution after incubation with sorted APC subsets for 3 days ($n = 4$ mice per group; $^*P < 0.05$). (**E**) In vivo proliferation of CFSE-labeled $CD90.1^+$ NR1 cells in a draining popliteal LN 3 days after footpad injection of APC subsets ($n = 4$ mice per group; $^*P < 0.05$). (**F**) FoxP3-eGFP–depleted NR1 cells were incubated in vitro with sorted APC subsets. Frequencies of FoxP3-$eGFP^+$ T_{regs} were determined by flow cytometry after 3 days ($n = 4$ mice per group; $^*P < 0.05$). (**G**) Eighteen hours after immunization, uterine DC subsets were analyzed by FACS for indicated markers ($n = 4$). Error bars represent mean ± SEM. Statistical differences were assessed using one-way ANOVA followed by Bonferroni posttest.

acquisition by a tolerogenic DC subset that expresses CD103, leading to the induction of T_{regs} that then shift the balance from protection to long-lived tolerance in the genital mucosa. Of note, a similar division of labor between $CD103^+$ and $CD103^-$ DCs has been described for the induction of intestinal tolerance and immunity, respectively (*49*). The differential Ag uptake by intestinal DC subsets is regulated by other mucosa-resident cell types (*50*–*52*); however, the mechanism(s) that regulate differential Ag acquisition by uterine DCs remain to be identified.

The route of administration determines UV-*Ct*–cSAP vaccine efficacy

Having established that targeting of uterine $CD103^-$ DCs by transcervical application of UV-*Ct*–cSAP generates long-term protection against genital *Ct* infection, we asked whether other routes of immunization could recapitulate this effect. Thus, mice were immunized with UV-*Ct*–cSAP either s.c. or intranasally (i.n.) and then challenged by i.u. *Ct* infection. Consistent with our experiments using mixtures of UV-*Ct* with conventional adjuvants (Fig. 1C), s.c. immunization with live *Ct* or UV-*Ct*–cSAP failed to protect (Fig. 6A). By contrast, exposure of nasopharyngeal mucosa to live *Ct* or UV-*Ct*–cSAP rendered mice resistant to genital *Ct* infection akin to i.u. immunization, and this cross-mucosal protective

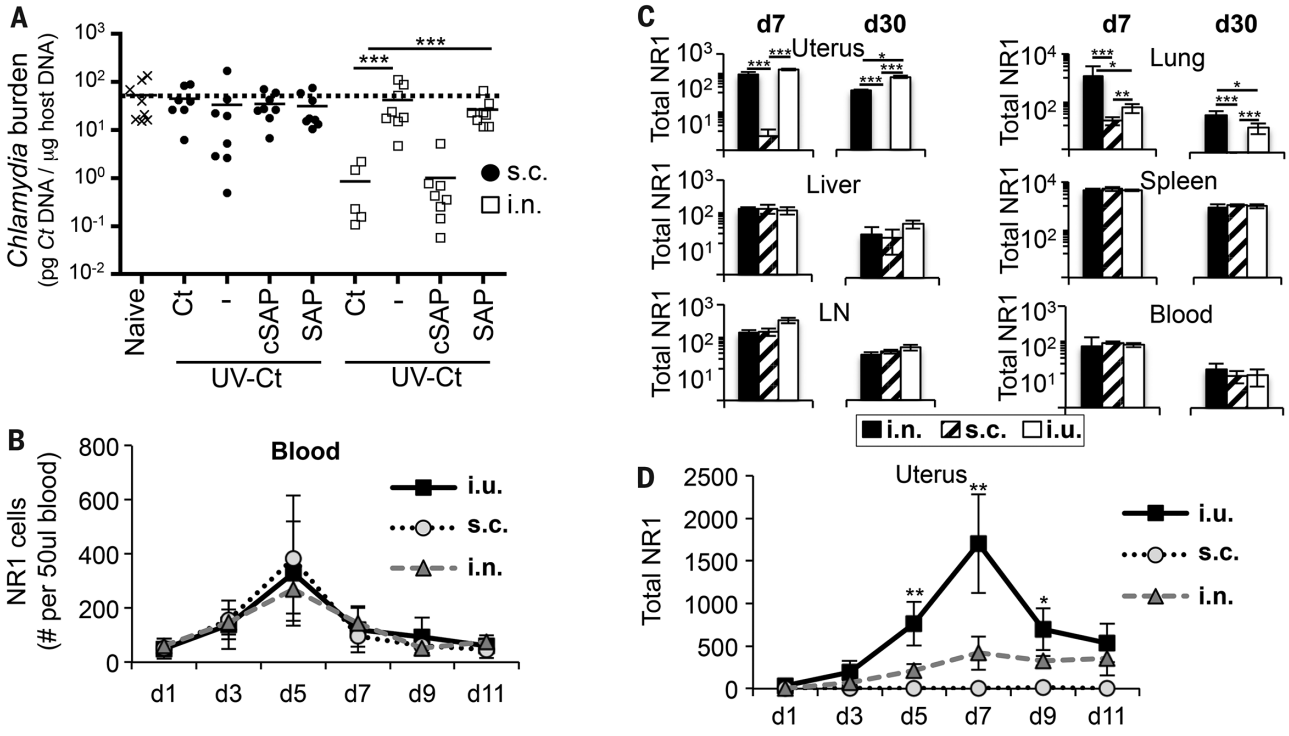

Fig. 6. Generation and protective function of uterus-resident and systemic memory T cell subsets induced by intranasal UV-*Ct*–cSAP vaccination. (**A**) *Ct* burden was determined by qPCR after i.u. *Ct* challenge 4 weeks after s.c. or i.n. immunization (n = 5 to 8 mice per group). (**B**) Time course of circulating NR1 T_{Eff} cells during days 1 to 11 after immunization (n = 4 mice per group). (**C**) Total number of NR1 cells recovered from indicated tissues on days 7 and 30 after i.n., s.c., or i.u. immunization. LN, mesenteric lymph node. (**D**) Time course of uterine NR1 cell accumulation during days 1 to 11 after immunization (n = 4 mice per group). (**E**) Schematic protocol for timed neutralization of α4 integrins in the three groups of *UV-Ct*–cSAP vaccinated mice shown in (F) and (G). (**F**) Total number of uterus-resident NR1 cells determined by flow cytometry (n = 4 mice per group). (**G**) Uterine *Ct* burden 3 days after i.u. *Ct* challenge. Data are from two independent experiments; n = 4 to 8 mice per group. Statistical differences were assessed using one-way ANOVA followed by Bonferroni posttest.

effect persisted unabated for at least 6 months (fig. S7). Interestingly, unlike i.u. conditioning with UV-*Ct*, neither i.n. nor s.c. exposure to UV-*Ct* enhanced the animals' susceptibility to genital *Ct* challenge, which suggests that the rules that govern regional immunity versus tolerance in the uterus may be distinct.

Rapid seeding of uterine mucosa with resident memory T cells (T_{RM} cells) after mucosal but not subcutaneous UV-*Ct*–cSAP vaccination

The fact that percutaneous immunization was ineffective, while vaccination via two distant mucosal routes generated potent protection against genital *Ct* infection, implied that protective CD4 T cells required priming in a MALT environment for efficient mucosal targeting (*12*). To further investigate this idea, we adoptively transferred 10^4 NR1 T_N cells into mice that were then immunized via different routes with UV-*Ct*–cSAP. Regardless of immunization route, the burst size of NR1 T_{Eff} cells in peripheral blood was equivalent in magnitude and peaked on day 5 (Fig. 6B). Similarly, 7 days and 30 days after i.n., s.c., or i.u. vaccination, NR1 cells were equally represented in blood, spleen, LNs, and liver, indicating that the route of immunization did not affect the differentiation or trafficking of T_{Eff} cells and memory cells to these nonmucosal sites (Fig. 6C). By contrast, i.u. and i.n. immunization generated Ag-experienced NR1 cells in the lung and uterus, while s.c. vaccination failed to generate mucosa-resident T_{Eff} cells (fig. S8, A to C). A closer examination of the kinetics of uterine T_{Eff} recruitment showed that NR1 T_{Eff} numbers increased gradually after i.n. vaccination, reaching a plateau on day 7. By contrast, i.u. vaccination resulted in a larger peak of uterus-resident NR1 cells on day 7 followed by contraction of the resident T cell pool over the next several days (Fig. 6D). By day 9, both mucosal vaccination strategies had elicited roughly similar uterus-resident T cell numbers, whereas NR1 cells remained essentially undetectable in uteri of s.c. immunized mice.

A critical protective role for uterine T_{RM} cells upon transcervical *Ct* challenge

The above results suggested that two distinct pools of *Ct*-specific memory T cells were induced: One population was modest in size and consisted

of mucosa-resident T_{RM} cells that arose from T_{Eff} cells that accessed the uterus early after mucosal (but not s.c.) priming. The pronounced spike in early NR1 T_{Eff} cell accumulation that was seen after i.u. (but not i.n.) vaccination was presumably a consequence of local tissue irritation that spurred inflammatory recruitment signals in the uterus. It is unlikely that i.n. vaccination altered the steady-state milieu in the uterus, so the fact that uterine T_{Eff} cell numbers increased steadily during the first 7 days after i.n. vaccination suggests the presence of constitutive mucosal recruitment signals for circulating T_{Eff} cells. Although the nature of these steady-state signals remains to be elucidated, our results indicate that T_{Eff} cells were selectively "imprinted" by mucosal (i.e., uterine or nasopharyngeal) APCs to engage this uterine recruitment pathway, whereas T_{Eff} cells generated in skin-draining LNs apparently lacked the prerequisite traffic molecule(s) for uterine homing. Moreover, the longevity of protection after i.n. vaccination (fig. S7) indicates that T_{Eff} cells that accessed the uterus gave rise to T_{RM} cells that persisted for at least six months without requiring the presence of local Ag.

The second vaccine-induced memory cell population was much larger than the number of uterus-resident T_{RM} cells and resided in blood and lymphoid tissues, where these cells are thought to survey the body for recall Ag (*53*). Although systemic memory cells were elicited by all immunization routes, their protective capacity may vary because of differential imprinting of mucosal homing pathways during the priming phase (*2*–*4*). For example, recent work has shown that protective CD4 T cells require the α4β1 integrin to access uterine mucosa (*54*). We made use of this fact to assess the relative contribution by each memory pool to the clearance of a recurrent *Ct* infection (Fig. 6E). To this end, we adoptively transferred NR1 T_N cells into three groups of mice that then received i.n. UV-*Ct*–cSAP vaccination. Three days later, when activated NR1 T_{Eff} first appeared in the blood, animals in group 1 were given rat IgG every 48 hours and served as controls in which memory cells had continuous access to the uterus; group 2 received injections of a blocking α4 integrin monoclonal antibody (mAb) every 48 hours, thus preventing uterine T cell homing throughout the experiment; group 3 received control IgG from day 3 to day 7, allowing the first wave of *Ct*-specific T_{Eff} cells to seed the uterine mucosa. On day 9, when i.n. vaccinated control mice had established a stable uterine T_{RM} cell pool (Fig. 6D), all groups were either challenged by i.u. inoculation of *Ct* or left unchallenged, and group 3 was then switched to treatment with α4 integrin mAb to prevent the secondary recruitment of circulating memory cells to the uterus. Animals were sacrificed on day 13 after immunization to assess uterine bacterial burden and/or NR1 cell distribution.

As expected (*54*), α4 integrin blockade in groups 2 and 3 profoundly affected the accumulation of both NR1 and endogenous CD4 T cells in the infected uterus but had no significant effect on CD4 T cells in the spleen (Fig. 6F and fig. S9, A to C). However, although continuous mAb treatment in group 2 essentially abrogated NR1 cell trafficking to both steady-state and infected uteri, the number of uterine NR1 cells in group 3 was significantly higher than in group 2 and equivalent to that in uninfected uteri of group 1. *Ct* infection in group 1 induced a factor of ~5 increase in uterine NR1 cells, whereas late inhibition of α4 integrins in group 3 completely prevented this secondary boost in uterine NR1 cell numbers. There was no difference between groups 1 and 3 in challenge-induced BrdU uptake or K_i-67 expression (a marker of ongoing cell division) by NR1 cells, indicating that mucosa-resident and newly recruited memory cells have a similar proliferative capacity (fig. S9D). Thus, the difference in mucosal T cell numbers between *Ct*-challenged animals in group 1 and group 3 likely reflects the α4 integrin–dependent influx of circulating T_{Eff} that occurred in response to infection-induced recruitment signals in the uterus (*9*). By contrast, the difference between groups 2 and 3 provides a measure for the number of vaccine-induced T_{Eff} that accessed the uterus early after priming and prior to *Ct* infection. Remarkably, although the total number of uterus-resident NR1 cells in group 3 was modest, the bacterial burden was reduced by an order of magnitude relative to naïve mice or animals in group 2, which remained completely unprotected (Fig. 6G). However, bacterial burdens in group 1 were even further reduced than in group 3, indicating that both tissue-resident and circulating T cells are needed to achieve optimal clearance of *Ct*. These findings confirm that the migration of both tissue-resident and circulating $CD4^+$ T cells into uterine mucosa depend on α4 integrins, presumably the α4β1 heterodimer (*54*). It is likely that additional trafficking molecules, such as chemokines, are involved in a tissue-specific multistep adhesion cascade for T cell recruitment to normal uterine mucosa (*53*), but the molecular identity of these constitutive traffic signals remains to be determined.

Circulating memory T cells induced by mucosal vaccination confer partial protection against *Ct* rechallenge

Having documented the protective capacity of mucosal T_{RM} cells, we next asked whether circulating memory cells can be protective in the absence of preexisting T_{RM} cells. To this end, we performed parabiosis surgery to generate pairs of congenic (CD45.1/CD45.2) mice, which establish a shared circulatory system, allowing genetically traceable hematopoietic cells from each animal to access the blood and tissues of a conjoined partner (*55*). Control experiments showed that CD4 T cell chimerism (the ratio of partner-derived:endogenous cells) in blood was minimal on day 3 after surgery but approached ~35:65 and 50:50 on days 4 and 5, respectively (fig. S10). Having thus determined that the earliest time point for circulating T cells to gain access to a parabiotic partner's tissues is on day ~4 after surgery, we performed a series of timed parabiosis experiments in congenic pairs of $CD90.2^+$ mice, whereby the $CD45.1^+$ animal in each pair was given genetically tagged ($CD90.1^+$) NR1 T_N cells, and both mice were immunized with UV-*Ct*–cSAP on the following day (day 0). Congenic pairs were subdivided into six groups: two groups underwent parabiosis surgery on day −14 or −1 before immunization, and four groups were parabiosed on day 1, 4, 14, or 21 after immunization (Fig. 7A). Six weeks after vaccination, the number of uterine NR1 T_{RM} cells was similar in all parabionts that had been conjoined on or before day 1 (Fig. 7B). In contrast, when parabiosis was initiated on day 4 or thereafter, the number of NR1 cells in uteri of nonimmunized $CD45.2^+$ partners of immunized $CD45.1^+$ animals was equivalent to that in completely naïve parabiotic pairs. These results imply that a transient wave of MALT-derived T_{Eff} cells gave rise to most, if not all, uterine T_{RM} cells within the first 7 days after immunization. Little or no further T cell recruitment to the uterus occurred after this time point. These findings are in perfect agreement with the time course of T_{Eff} cell accumulation in uteri of conventional mice, which increased until day 7 and plateaued thereafter (Fig. 6D).

To assess the protective capacity of the circulating memory subset, we devised a modification of the above protocol (Fig. 7C), whereby two groups of congenic mice were paired and each $CD45.2^+$ partner received 10^5 NR1 T_N cells followed by i.n. UV-*Ct*–cSAP vaccination. Animals in group A were vaccinated 2 weeks after parabiosis, while in group B, vaccination preceded parabiosis by 2 weeks. After another 2 weeks, both partners were challenged with *Ct*. Four days later, infected uteri in both vaccinated and naïve parabiotic animals had recruited substantial numbers of *Ct*-specific NR1 cells (Fig. 7, D and E) that exceeded those recovered from uninfected uteri of vaccinated mice (Figs. 6D and 7B). Uterine NR1 cell recruitment was markedly enhanced in all parabionts in group A, where *Ct*-specific memory cells had been generated after a shared circulation was already established so NR1 T_{RM} cells could seed uteri of both partners (Fig. 7D). By contrast, in group B, parabiosis was performed after the early wave of mucosa-seeding T_{Eff} cells had subsided, so uterus-resident NR1 T_{RM} cells were restricted to the immunized $CD45.2^+$ partner (Fig. 7E), whereas circulating memory cells could equilibrate between both partners. Consequently, both parabionts in group A were effectively protected against genital *Ct* challenge (Fig. 7F). By contrast, in group B, only the immunized partners were fully protected, while the bacterial burden in nonimmunized animals, which harbored only circulating NR1 memory cells, were indistinguishable from naïve NR1 recipients (Fig. 7G). Of note, UV-*Ct*–cSAP vaccination induced a robust humoral response against *Ct* (fig. S3A), whereby circulating antibodies are expected to fully equilibrate in parabiotic pairs. The preferential protection of only the vaccinated parabionts in group B suggests that antibodies provided little or no protection in this experimental setting.

Although the above experiments permitted simultaneous assessment of the migratory dynamics

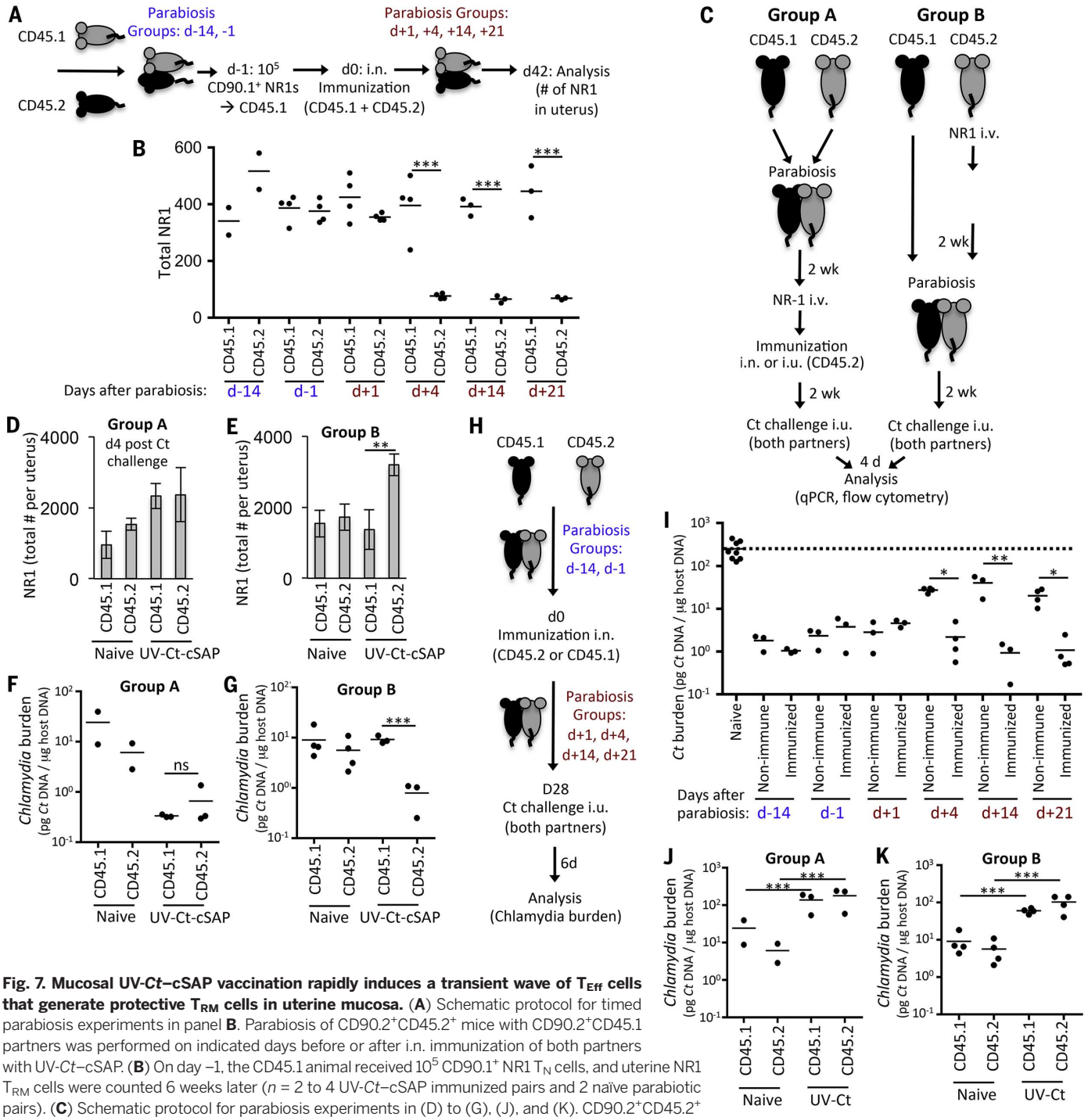

Fig. 7. Mucosal UV-*Ct*–cSAP vaccination rapidly induces a transient wave of T_{Eff} cells that generate protective T_{RM} cells in uterine mucosa. (**A**) Schematic protocol for timed parabiosis experiments in panel **B**. Parabiosis of CD90.2$^+$CD45.2$^+$ mice with CD90.2$^+$CD45.1 partners was performed on indicated days before or after i.n. immunization of both partners with UV-*Ct*–cSAP. (**B**) On day –1, the CD45.1 animal received 10^5 CD90.1$^+$ NR1 T_N cells, and uterine NR1 T_{RM} cells were counted 6 weeks later (n = 2 to 4 UV-*Ct*–cSAP immunized pairs and 2 naïve parabiotic pairs). (**C**) Schematic protocol for parabiosis experiments in (D) to (G), (J), and (K). CD90.2$^+$CD45.2$^+$ mice were immunized with UV-*Ct*–cSAP i.n. or UV-*Ct* i.u. 2 weeks before or after parabiosis with a CD90.2$^+$CD45.1 partner. 1 × 10^5 CD90.1$^+$ NR-1 T_N were adoptively transferred to the CD45.2$^+$ animal one day prior to immunization. Animals were either immunized 2 weeks after [group A; (D), (F), (J)] or two weeks before parabiosis surgery [group B; (E), (G), (K)]. n = 3 parabiotic pairs immunized with UV-*Ct*–cSAP or UV-*Ct* and 2 naïve parabiotic pairs. (**D** and **E**) Total number of NR1 cells in the uterus 4 days after *Ct* challenge (n = 3 parabiotic pairs immunized with UV-*Ct*–cSAP and 2 naïve parabiotic pairs. $^{**}P < 0.01$). (**F** and **G**) *Ct* burden 4 days after i.u. *Ct* challenge of both partners in animals that had been conditioned with i.n. UV-*Ct*–cSAP. (**H**) Schematic protocol for timed parabiosis experiments in (I). One partner of each CD45.1/CD45.2 congenic pair was randomly chosen to be immunized on day 0 and underwent parabiosis surgery at indicated time points. (**I**) Both parabionts in each pair (n = 3 or 4 per group) were challenged i.u. with *Ct* on day 28. Nonimmunized parabiotic pairs served as naïve controls (n = 4). *Ct* burden was assessed 6 days after challenge. All groups were significantly different from naïve parabionts ($P < 0.05$; one-way ANOVA followed by Bonferroni posttest.). (**J** and **K**) Uterine *Ct* burden 4 days after both i.u. *Ct* challenge of parabiotic partners after conditioning with i.n. UV-*Ct*. $^{***}P < 0.001$; ns, nonsignificant. Error bars show mean ± SEM. Unless stated otherwise, statistical differences were assessed using two-tailed t test.

and protective function of *Ct*-specific T cells, the experimental protocol required NR1 T_N cells to be transferred at superphysiologic numbers. To control for potential artifacts of elevated frequencies of *Ct*-specific T cells, we performed timed parabiosis experiments without NR1 cell transfer. To this end, either the CD45.1$^+$ or CD45.2$^+$ partner of each congenic pair was immunized before or after parabiosis surgery, and both animals were challenged 4 weeks later with *Ct* i.u. (Fig. 7H). When uterine bacterial burden was assessed 6 days later, both partners were fully protected when parabiosis had been performed on or before day 1 after vaccination (Fig. 7I). Thus, mucosal UV-*Ct*–cSAP vaccination of animals that could generate both T_{RM} and circulating memory cells elicited similar protection against *Ct* challenge with and without prior adoptive transfer of TCR transgenic NR1 cells and regardless of whether we examined individual mice (compare Fig. 2A and Fig. 6G) or

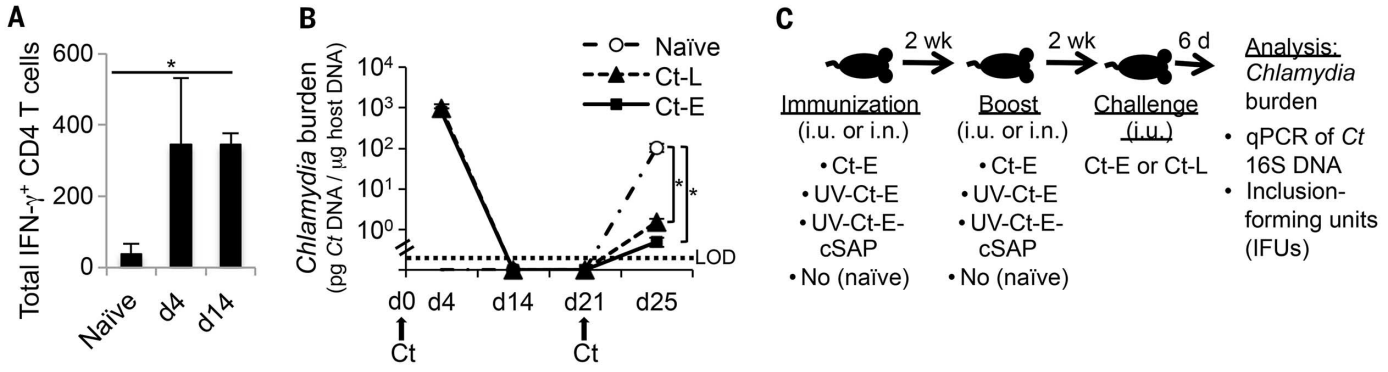

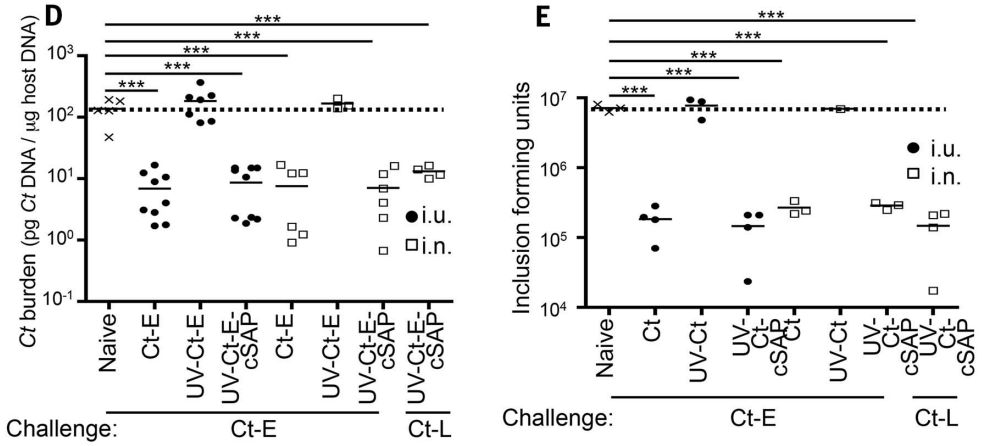

Fig. 8. Humanized BLT mice are protected from *Ct* challenge after UV-*Ct*–cSAP immunization. (**A** and **B**) Immune response of a cohort of humanized BLT mice to uterine infection with *Ct-E* or *Ct-L*. All animals had been reconstituted with human fetal thymus, liver, and hematopoietic stem cells from the same donor. (A) Number of IFN-γ–producing human CD4 T cells per uterus ($n = 5$ mice per time point; $^*P < 0.05$). (B) Animals were infected on day 0 and rechallenged on day 21 (arrows). Uterine *Ct* burden was measured on days 4, 14, 21, or 25 by qPCR. LOD, limit of detection; *Ct-E*, *C. trachomatis* serotype E; *Ct-L*, *C. trachomatis* serotype L. $n = 2$ mice per group. $^*P < 0.05$. (**C**) Schematic protocol for experiments in (D) and (E). These experiments were performed using two cohorts of BLT mice that had been reconstituted with material from different human donors. (**D** and **E**) BLT mice were left naïve or immunized (day 0) and boosted (day 14) as indicated using *Ct* serotype E (*Ct*-E) as immunogen. All animals were challenged with live *Ct*-E or *Ct* serotype L (*Ct*-L) on day 28. *Ct* burden was determined (D) by qPCR or (E) by measurement of IFUs on day 6 after challenge ($n = 1$ to 9 mice per group pooled from two independent experiments with material from genetically different human donors). $^*P < 0.05$, $^{**}P < 0.01$, $^{***}P < 0.001$; ns, not significant. Error bars reflect mean ± SEM. (**F**) Schematic summary conclusion. Two waves of vaccine-induced *Ct*-specific memory T cells must access the uterine mucosa to confer optimal protection against *Ct* challenge. Mucosal vaccination against *Ct* induces an early burst of circulating T_{Eff} cells (solid lines) that seed the uterine mucosa during the first week after immunization (wave 1) and give rise to long-lived resident memory T cells. By contrast, nonmucosal vaccines do not induce this first wave of mucosa-tropic memory cells (broken lines). Regardless of vaccination route, immunized hosts generate circulatory memory T cells, which do not traffic to resting uterine mucosa and are slow to access the rechallenged uterus in the absence of preexisting T_{RM} cells. However, in mucosal vaccine recipients, uterine T_{RM} cells can respond instantly to rechallenge with *Ct* and instigate the rapid recruitment of additional *Ct*-specific memory cells from the circulating pool (wave 2). Our results indicate that memory cells from both waves are required for optimal clearance of uterine *Ct* infection. Statistical differences were assessed using one-way ANOVA followed by Bonferroni posttest.

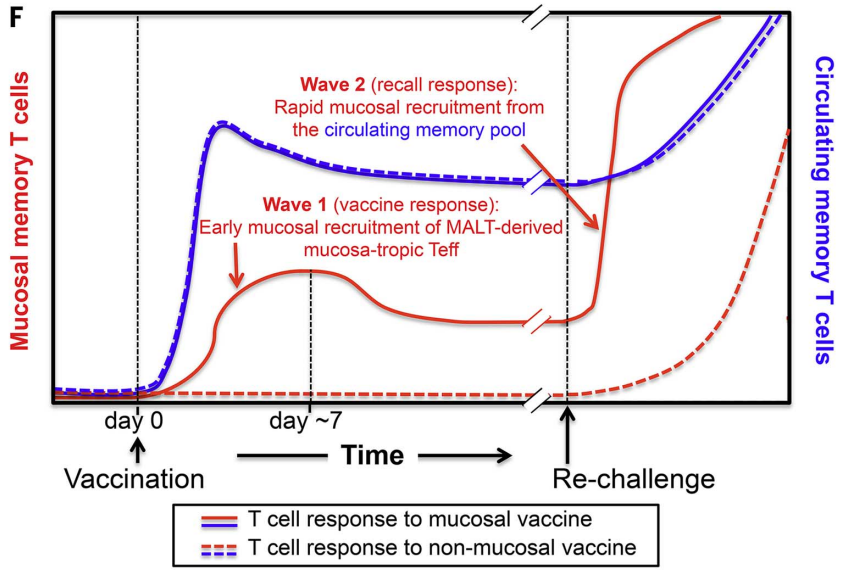

parabiotic pairs (compare Fig. 7, B and D), indicating that NR-1 cell transfers did not artificially skew the overall vaccine response.

Importantly, when parabiosis was delayed until day 4 or later after vaccination, protection of the nonimmunized parabionts was noticeably compromised. These findings strongly support the notion that mucosal seeding by vaccine-induced T_{RM} cells must occur after day 8 after vaccination (Fig. 7B) and is essential for full-fledged resistance to genital *Ct* challenge. However, even when parabiosis of animals that did not receive NR1 T_N cells was delayed after vaccination until day 4 or later, subsequent *Ct* challenge of nonimmunized partners resulted in significantly lower bacterial burdens than when naïve parabionts were challenged (Fig. 7I). Thus, the circulating memory cells that arose from a polyclonal T cell response provided meaningful, if partial, protection in the absence of T_{RM} cells, while the analogous experiment after adoptive transfer of NR1 T_N failed to reveal protection by circulating memory cells (Fig. 7G). This difference was presumably because conventional naïve mice contain much fewer *Ct*-specific T_N than NR1 cell recipients, allowing the latter to rapidly generate a large burst of T_{Eff} cells after *Ct* challenge that may have masked the activity of circulating memory cells. In aggregate, our results suggest that circulating polyclonal memory T cells that arise after mucosal vaccination can accelerate uterine *Ct* clearance, even in the absence of mucosal T_{RM} cells. However, consistent with the partial protection afforded by adoptive transfer of sensitized splenic CD4 T cells (Fig. 3B), this protective activity is suboptimal.

Mucosal UV-*Ct* exposure generates suppressive T_{regs} in parabiotic partners

Finally, we examined parabiotic pairs in which the CD45.2$^+$ partner had received i.u. conditioning with UV-*Ct*. Remarkably, both partners displayed similar hypersusceptibility to *Ct* regardless of whether parabiosis was initiated before or after UV-*Ct* immunization (Figs. 7J, K), indicating that uterus-resident T_{regs} may not be needed for the tolerogenic response to *Ct*. This is in line with observations in a murine colitis model, where tissue-homing of T_{regs} was not required to prevent intestinal inflammation (*56*).

Mucosal UV-*Ct*–cSAP vaccination confers protection against *Ct* challenge in humanized mice

The above findings in conventional mice were fully reproducible in two cohorts of BLT mice (*57*) that had been reconstituted with a human immune system from two unrelated donors (*58*). Human CD4 T cells in both cohorts mounted a vigorous mucosal T_H1 response to clear uterine infection with two different *Ct* serovars, *Ct-L* and *Ct-E* (Fig. 8, A and B). Moreover, prime-boost vaccination of naïve BLT animals with UV-*Ct*–cSAP given i.n. or i.u. (Fig. 8C) was highly effective against subsequent i.u. *Ct* challenge, even when BLT mice were challenged with a different serotype than used for immunization (Fig. 8, D and E).

Conclusion

Using a mucosal immunization strategy, we have dissected the multifaceted adaptive immune mechanisms that control murine host responses against genital *Ct* infection after mucosal vaccination with a vaccine candidate, UV-*Ct*–cSAP. Our results indicate that optimal protection after *Ct* challenge requires uterine recruitment of two discrete waves of *Ct*-specific CD4 T cells that are inducible in MALT but not in skin-draining LNs (Fig. 8F). After an immunostimulatory mucosal priming event, the first wave is composed of recently activated T_{Eff} cells that give rise to long-lived T_{RM} cells after trafficking to both inflamed and resting mucosal surfaces. This early migratory wave subsides within ~1 week after immunization and depends on a constitutive tissue-specific multistep adhesion cascade (*53*) involving α4 integrins and presumably other mucosal traffic signals that remain to be identified. Concomitantly, MALT-derived *Ct*-responsive T_{Eff} cells also generate a second population of memory cells that preferentially reside in blood and secondary lymphoid organs. This systemic memory population, which comprises the two classical central and effector memory subsets (*59*), does not appear to access the resting urogenital mucosa but can be recruited to peripheral tissues (including uterine mucosa) upon the onset of inflammation (*60*). Although this circulating memory subset contributes to the overall recall response against *Ct*, its protective role is suboptimal in the absence of T_{RM} cells. In an optimally immunized individual, *Ct* infection triggers rapid release of cytokines, particularly IFN-γ, by the mucosal T_{RM} subset, which promotes pathogen clearance (*61*). This protective effect of uterine T_{RM} may be amplified by their proinflammatory activity that may help recruit circulating memory cells; however, our data show that the tissue-resident memory subset confers substantial protection even when the influx of circulating memory cells is blocked.

Of importance to future *Ct* vaccine trials, our experiments potentially shed light on the decades-old conundrum of how exposure to killed *Ct* in trachoma vaccine trials during the 1960s may have enhanced subsequent *Ct*-induced pathology (*25*–*29*). We could provoke a similar hypersusceptibility to *Ct* in our mouse model by exposing mucosal surfaces to UV-*Ct*, an effect that was due to de novo induction of *Ct*-specific T_{regs}. After conjugating cSAPs to UV-*Ct* for mucosal immunization, we not only could prevent this tolerogenic effect but also could render mice highly resistant to *Ct* infection—a protective response that was identical in magnitude, longevity, and immunological mechanism to the endogenous memory response against genuine *Ct* infection. Moreover, our findings in BLT mice indicate that human CD4 T cells can also mount a vigorous mucosal T_H1 response to clear uterine *Ct* infection, which suggests that cSAP-based mucosal vaccination may also elicit protective immune responses in humans. Because cSAPs are fully synthetic and biodegradable nanoparticles that are easily manufactured and well tolerated, they may also offer a powerful and versatile approach for mucosal vaccine development against other challenging pathogens.

Materials and methods

Mice

C57BL/6 and BALB/c mice, 6 to 8 weeks old, were purchased from Charles River or The Jackson Laboratory. B6.129S2-H2$^{dlAb1\text{-}Ea}$/J (referred to as MHC class II$^{-/-}$) (*48*), *CD8*$^{-/-}$, μMt, *Il10*$^{-/-}$, *Rag2*$^{-/-}$, and C57BL*6* B6.SJL Ptprca Pep3b/BoyJ (CD45.1$^+$) mice were purchased from The Jackson Laboratory and used at 6 to 12 weeks of age. CD90.1 NR1 mice (TCR tg mice with specificity for the CD4$^+$ T cell antigen *Cta*1 from *Ct*) were bred in-house. For some experiments, we crossed NR1 and Foxp3eGFP mice (*62*). For characterization of uterine APC subsets, CXCR3$^{GFP/+}$ mice (*63*) were used. BLT mice were generated in the MGH Humanized Mouse Program by transplanting irradiated *NOD/SCID/*$\gamma c^{-/-}$ mice with human fetal liver stem cells and autologous thymic grafts (*57*). Reconstituted mice developed a fully human lymphoid compartment within ~13 to 18 weeks after reconstitution, at which stage they were used for immunization or vaccination studies. All experiments were performed in accordance with NIH guidelines and approved by the Institutional Animal Committees of Harvard Medical School and MGH.

Chlamydia infection and detection

Ct serovar L2 (434/Bu), referred to as *Ct*, or serovar E (*Ct-E*) or *C. muridarum* (*Cm*) were propagated in McCoy cell monolayers grown in Eagle's MEM (Invitrogen, Grand Island, NY) supplemented with 10% FCS, sodium bicarbonate (1.5 g/liter), 0.1 M nonessential amino acids, and 1 mM sodium pyruvate, as described (*41*). Aliquots were stored at −80°C in medium containing 250 mM sucrose, 10 mM sodium phosphate, and 5 mM L-glutamic acid and were thawed immediately before use. All mice were treated with 2.5 μg of medroxyprogesterone s.c. 7 days before immunization to normalize the murine estrous cycle. For UV inactivation, *Ct* or *Cm* suspensions were placed under a UV lamp (15 W) at a distance of 30 cm for 30 min. The efficiency of UV inactivation was always tested by infecting McCoy cell monolayers with an aliquot of UV-inactivated Ct and evaluation of inclusion-forming units. Briefly, 30 hours after infection, the medium was removed, and cells were fixed in ice-cold methanol and permeabilized in PBS with 0.05% tween. Cells were then stained with 10 μl of anti-MOMP antibody and Evans blue counterstain (Pathfinder Diagnostic Kit BioRad) for 1 hour and were then washed three times in PBS-tween. Inclusion-forming units were not observed after UV inactivation of *Ct* or *Cm*.

Intrauterine immunization and challenge were conducted transcervically using an NSET

device (ParaTechs) as described (*31*). Briefly, 10 μl of sucrose-phosphate-glutamate medium containing 10^6 *Ct* or UV-*Ct* ± cSAP was placed into the uterus using the NSET pipet tip through the NSET speculum. Subcutaneous immunization was done with a U-100 insulin syringe injecting 10 μl of sucrose-phosphate-glutamate medium containing 10^6 *Ct* or UV-*Ct* ± cSAP. As 10^6 *Ct* were lethal for mice when deposited intranasally, i.n. immunization was performed with 10^5 *Ct* in 10 μl of sucrose-phosphate-glutamate medium. *Cm* was administered intravaginally as described previously (*6*).

To quantify the levels of *Ct* in tissues, we usually used qPCR with 16S primers specific for *Ct*, as described previously (*64*). Briefly, DNA was isolated from uterus homogenates using the QIAamp DNA mini kit (Qiagen). Mouse GAPDH DNA and *Chlamydia* 16S DNA were quantified by qPCR on an ABI Prism 7000 sequence detection system. Using standard curves from known amounts of *Ct* and mouse DNA, the amount of *Chlamydia* DNA (in pg) per unit weight of mouse DNA (in μg) was calculated to assess bacterial burden.

Titers of inclusion-forming units were determined in two experiments. Mouse uteri were disrupted using a tissue homogenizer and frozen at −80°C. Aliquots were thawed, and tenfold dilutions of each sample were made in a 96-well plate. Each dilution was then used to infect a confluent monolayer of McCoy cells in a 96-well plate by centrifugation for 1 hour at 37°C. Two hours after centrifugation, medium was supplemented with gentamicin (25 μg/ml) to prevent contamination. Thirty hours after infection, the media was removed, and cells were fixed in ice-cold methanol and permeabilized in PBS with 0.05% tween. Cells were then stained with 10 μl of anti-MOMP antibody and Evans blue counterstain (Pathfinder Diagnostic Kit BioRad) for 1 hour and then were washed three times in PBS-tween. Total inclusions in each sample were then enumerated by fluorescence microscopy, with at least three fields being counted per sample.

The impact of the cSAP constructs on chlamydia-induced pathology of the upper genital tract was measured 4 weeks after Cm challenge of immunized mice and naïve controls. Gross pathology was scored by hydrosalpinx development as follows: 0: normal; 1: low-level fluid in oviduct; 2: moderate amount of fluid present; 3: high level of fluid.

Vaccine formulation

Synthesis of polymers and formulation of synthetic nanoparticles (SPs) was performed as described previously (*32*) with minor modifications. Briefly, the triblock copolymer poly(D,L-lactic-*co*-glycolic acid)-*b*-poly(l-histidine)-*b*-poly(ethylene glycol) (PLGA-PLH-PEG, referred to as charge-switching synthetic particles, cSPs) was synthesized using a polymer end grafting strategy. Control SPs that lacked the PLH block were formulated in a similar manner using PLGA-PEG copolymers. R848-PLA was synthesized by ring-opening polymerization (*33*). All SPs were formulated using a modified emulsion/solvent evaporation technique. R848-PLA was added in a 0.4:0.4:0.2 (R848-PLA: PLGA-PLH-PEG:PLGA-PEG) ratio. The polymer-containing ethyl acetate solution was sonicated into 2 ml of pure water using a probe tip sonicator (Misonix Sonicator S-4000, Farmingdale, NY) for 30 s in continuous mode at 40% amplitude and then diluted into 8 ml of pure water under magnetic stirring in a fume hood. The solvent was allowed to evaporate for at least 2 hours, at which point SPs were collected and purified by repeated ultrafiltration using Amicon Ultra-4 100,000 NMWL cutoff filters (Millipore, Billerica, MA). The sizes of *Ct*-SP constructs were determined by dynamic light scattering on a Zetasizer Nano (Malvern Instruments).

SAPs, cSAPs, and cSPs were prepared, purified, and then resuspended in a dilute pH 6.0 solution, and 2×10^7 UV-*Ct* were added per mg SPs. This mixture was then incubated at 37°C for at least 30 min in the dark under gentle shaking. To determine SP conjugation to the surface of UV-*Ct*, Ct was labeled with BacLight (Life Technologies, absorption maximum 581, emission maximum 644) and PLGA-AF488, synthesized using ring-opening polymerization, was blended in to the SPs prior to conjugation with bacteria and analyzed with flow cytometry.

Tissue digestion, flow cytometry, and cell sorting

Spleens, lungs, lymph nodes, and livers were cut into small pieces with a sterile scalpel and passed through 40-μm mesh filters. Uteri were digested with type XI collagenase (Sigma, St Louis, MO) and DNase I (Sigma) for 30 min at 37°C before passing through 40-μm filters. Samples were enriched for lymphocytes by density-gradient centrifugation with NycoPrep 1.077 according to the manufacturer's protocol (Axis-Shield).

For flow cytometry analysis or cell sorting, T cells were stained with anti-CD3e (145-2C11; BioLegend), anti-CD4 (RM4-5; BioLegend), anti-CD90.1 (OX-7; BioLegend), anti-CD25 (PC61; BioLegend), anti-Vα2 (B20.1; BioLegend), anti-Vβ8.3 (1B3.3; BD Biosciences), anti-CD45.1 (104; BioLegend), or anti-CD45.2 (A20; BioLegend). T cell proliferation was measured by anti-K_i-67 (16A8; BioLegend) staining and overnight bromodeoxyuridine (BrdU) labeling according to the manufacturer's protocol (Life Technologies). DCs were characterized and/or sorted with anti-MHC class II (AF6-120.1; BioLegend), anti-F4/80 (BM8; BioLegend), anti-CD103 (2E7; BioLegend), anti-CD11c (N418; BioLegend), anti-CD11b (M1/70; BioLegend), anti-CD207 (eBioL31; eBioscience), anti-CD301b (URA-1; BioLegend), anti-CD80 (16-10A1; BioLegend), anti-CD86 (GL-1; BioLegend), anti-CD274 (PD-L1) (10F.9G2; BioLegend), anti-CD273 (PD-L2) (TY25; BioLegend), anti-IL-10 (JES5-16E3; BioLegend), and anti-IL-12/IL-23 (C15.6; BioLegend). For intracellular T cell cytokine staining, autologous sorted splenic $CD11c^+$ DCs were pulsed with UV-inactivated EBs for 30 min, washed extensively, and added to T cells for 5 hours in the presence of brefeldin A (GolgiStop; BD Biosciences). T cells were stained for anti–IFN-γ (XMG1.2; BioLegend), anti–IL-2 (JES6-5H4; BioLegend), and anti–TNF-α (MP6-XT22; BioLegend) Abs after permeabilization with the Cytofix/Cytoperm Plus Kit according to the manufacturer's instructions (BD Biosciences). The absolute cell number in each sample was determined using AccuCheck Counting Beads (Invitrogen). Data were collected on a FACSCanto (BD Biosciences) or a LSRII (BD Biosciences) and analyzed using FlowJo 9.3.2. A FACSAria (BD) was used for cell sorting with Diva software, and purity was >98% for all experiments.

Adoptive transfer of leukocyte subsets

Lymph nodes and spleens were collected from naïve female $CD90.1^+$ NR1 mice and purified by negative immunomagnetic cell sorting using a mouse $CD4^+$ T cell isolation kit (~98% $CD4^+$, Miltenyi Biotec). Purity was verified with anti-CD4, anti-Vα2, and anti-Vβ8.3 stainings. For some experiments, $FoxP3^{eGFP+}$ NR1 cells were depleted before adoptive transfer of $FoxP3^{eGFP-}$ NR1 cells by cell sorting. 10^5 isolated NR1 cells (unless noted elsewise) were intravenously transferred to naïve recipient mice 1 day prior to immunization. In proliferation experiments, NR1 cells were labeled with carboxyfluorescein succinimidyl ester (CFSE) before transfer. For adoptive transfer of polyclonal $CD4^+$ and $CD8^+$ T cells and T cell–depleted leukocytes, cell subsets from immunized mice were harvested from donor spleens by immunomagnetic cell sorting (Miltenyi Biotec), and 10^7 cells were transferred to naïve recipients.

NR1 T cell stimulation by APCs

APCs were isolated from single-cell suspensions of uterus and draining LNs 18 and 24 hours after immunization, respectively. $CD45^+$MHC class II^+ cells were FACS sorted based on their CD103 and F4/80 expression ($CD103^-F4/80^+$ macrophages, $CD103^-F4/80^-$ DCs, and $CD103^+F4/80^-$ DCs). Sorted cells were either subjected to qPCR analysis for *Ct* 16S content or cocultured with CFSE-labeled NR1 cells for 3 days (500 DCs and 5000 NR-1 cells). For in vivo assessment of APC function, naïve mice received 10^5 CFSE-labeled NR1 cells i.v. followed one day later by s.c. injection into the right footpad of 5000 sorted APCs. CFSE dilution of NR1 cells in the right popliteal LN was analyzed 3 days later.

In vivo mAb treatment

Two hundred fifty μg anti-CD25 (PC61) mAb or control IgG were administered intraperitoneally at days −3 and +3 of uterine *Ct* challenge. Anti-α4 mAb (PS/2) or control IgG was administered i.v. at day 3 (100 μg) and every second day (50μg) until day 11 thereafter. On d9, mice were challenged i.u. with 10^6 IFU of *Ct*.

Parabiosis

Parabiosis surgery was performed as previously described (*55*). Briefly, sex- and weight-matched congenic partners were anaesthetized with ketamine (100 mg/kg body weight) and xylazine (10 mg/kg body weight) by i.p. injection. The corresponding lateral aspects of mice were shaved, and the excess hair was wiped off with an alcohol prep pad.

Two matching skin incisions were made from the olecranon to the knee joint of each mouse, and the subcutaneous fascia was bluntly dissected to create about 0.5 cm of free skin. The olecranon and knee joints were attached by a double 4-0 braided silk suture and tied, and the dorsal and ventral skins were approximated by staples or continuous 6-0 braided silk suture. The mice were then kept on heating pads and continuously monitored until recovery. Flunixin (2.5 $\mu g\ g^{-1}$) and buprenorphine (0.05 to 0.1 mg/kg body weight) were used for analgesic treatment by subcutaneous injection after the operation. After 3 days to 2 weeks, chimerism of leukocytes from the blood was monitored to ensure equivalent blood exchange between parabiotic partners. Depending on the readout of the experiments, either one of the partners was immunized with UV-*Ct*–cSAP i.n. or UV-*Ct* i.u. and both were challenged with *Ct* i.u., or 10^5 NR1 cells were i.v. injected the day before immunization with UV-*Ct*–cSAP i.n. without further challenge.

*Anti-*Ct *Ab ELISA*

Antibody levels were determined by enzyme-linked immunosorbent assays (ELISA) using a mouse *Ct* antibody ELISA Kit (MyBioSource). Mice were bled 4 weeks after immunization in order to assess antibody levels.

Confocal and electron microscopy

Uterine tissue was incubated overnight in phosphate-buffered L-lysine with 1% paraformaldehyde/periodate and then cryoprotected by subsequent incubations in 10%, 20%, and 30% sucrose in PBS at room temperature, snap-frozen in TBS tissue-freezing liquid (Triangle Biomedical Sciences), and stored at −80°C. Sections of 30-μm thickness were mounted on Superfrost Plus slides (Fisherbrand) and stained with anti-CD90.1 PE (OX-7, BD Biosciences), anti-CD326 FITC (G8.8: BioLegend), and anti-CD31 (390, BioLegend) in a humidified chamber after Fc receptor blockade with antibody 2.4G2 (BD Pharmingen, 1 μg/ml). Samples were mounted in FluorSave reagent solution (EMD-Calbiochem) and stored at 4°C until analysis. Images were acquired with an Olympus Fluoview BX50WI inverted microscope and were analyzed by using Volocity software (Improvision).

Transmission electron microscopy (TEM) samples were prepared using the Gatan Cryo-Plunge3 and imaged using a JEOL 2100 FEG electron microscope.

Statistical analysis

Statistical significance was determined between two groups with two-tailed *t*-test. Statistical differences among three or more groups were assessed using one-way or two-way analysis of variance (ANOVA) followed by Bonferroni posttest to account for multiple comparisons. Significance was set at a P value of less than 0.05.

REFERENCES AND NOTES

1. J. Holmgren, A. M. Svennerholm, Vaccines against mucosal infections. *Curr. Opin. Immunol.* **24**, 343–353 (2012). doi: 10.1016/j.coi.2012.03.014; pmid: 22580196
2. J. R. Mora *et al*., Selective imprinting of gut-homing T cells by Peyer's patch dendritic cells. *Nature* **424**, 88–93 (2003). doi: 10.1038/nature01726; pmid: 12840763
3. J. R. Mora *et al*., Generation of gut-homing IgA-secreting B cells by intestinal dendritic cells. *Science* **314**, 1157–1160 (2006). doi: 10.1126/science.1132742; pmid: 17110582
4. H. Sigmundsdottir *et al*., DCs metabolize sunlight-induced vitamin D3 to 'program' T cell attraction to the epidermal chemokine CCL27. *Nat. Immunol.* **8**, 285–293 (2007). doi: 10.1038/ni1433; pmid: 17259988
5. D. Guy-Grand, C. Griscelli, P. Vassalli, The mouse gut T lymphocyte, a novel type of T cell. Nature, origin, and traffic in mice in normal and graft-versus-host conditions. *J. Exp. Med.* **148**, 1661–1677 (1978). doi: 10.1084/jem.148.6.1661; pmid: 31410
6. A. Kantele, J. Zivny, M. Häkkinen, C. O. Elson, J. Mestecky, Differential homing commitments of antigen-specific T cells after oral or parenteral immunization in humans. *J. Immunol.* **162**, 5173–5177 (1999). pmid: 10227989
7. D. J. Campbell, E. C. Butcher, Rapid acquisition of tissue-specific homing phenotypes by $CD4^+$ T cells activated in cutaneous or mucosal lymphoid tissues. *J. Exp. Med.* **195**, 135–141 (2002). doi: 10.1084/jem.20011502; pmid: 11781372
8. J. M. Schenkel, K. A. Fraser, V. Vezys, D. Masopust, Sensing and alarm function of resident memory CD8 T cells. *Nat. Immunol.* **14**, 509–513 (2013). doi: 10.1038/ni.2568; pmid: 23542740
9. J. M. Schenkel *et al*., T cell memory. Resident memory CD8 T cells trigger protective innate and adaptive immune responses. *Science* **346**, 98–101 (2014). doi: 10.1126/science.1254536; pmid: 25170049
10. T. Gebhardt *et al*., Memory T cells in nonlymphoid tissue that provide enhanced local immunity during infection with herpes simplex virus. *Nat. Immunol.* **10**, 524–530 (2009). doi: 10.1038/ni.1718; pmid: 19305395
11. T. Bergsbaken, M. J. Bevan, Proinflammatory microenvironments within the intestine regulate the differentiation of tissue-resident $CD8^+$ T cells responding to infection. *Nat. Immunol.* **16**, 406–414 (2015). doi: 10.1038/ni.3108; pmid: 25706747
12. J. Bienenstock, The mucosal immunologic network. *Ann. Allergy* **53**, 535–540 (1984). pmid: 6391284
13. W. S. Gallichan, K. L. Rosenthal, Long-lived cytotoxic T lymphocyte memory in mucosal tissues after mucosal but not systemic immunization. *J. Exp. Med.* **184**, 1879–1890 (1996). doi: 10.1084/jem.184.5.1879; pmid: 8920875
14. M. Santosuosso *et al*., Mechanisms of mucosal and parenteral tuberculosis vaccinations: Adenoviral-based mucosal immunization preferentially elicits sustained accumulation of immune protective CD4 and CD8 T cells within the airway lumen. *J. Immunol.* **174**, 7986–7994 (2005). doi: 10.4049/jimmunol.174.12.7986; pmid: 15944305
15. H. K. Lee *et al*., Differential roles of migratory and resident DCs in T cell priming after mucosal or skin HSV-1 infection. *J. Exp. Med.* **206**, 359–370 (2009). doi: 10.1084/jem.20080601; pmid: 19153243
16. H. Shin, A. Iwasaki, A vaccine strategy that protects against genital herpes by establishing local memory T cells. *Nature* **491**, 463–467 (2012). doi: 10.1038/nature11522; pmid: 23075848
17. N. Lycke, Recent progress in mucosal vaccine development: Potential and limitations. *Nat. Rev. Immunol.* **12**, 592–605 (2012). doi: 10.1038/nri3251; pmid: 22828912
18. F. W. van Ginkel *et al*., Enterotoxin-based mucosal adjuvants alter antigen trafficking and induce inflammatory responses in the nasal tract. *Infect. Immun.* **73**, 6892–6902 (2005). doi: 10.1128/IAI.73.10.6892-6902.2005; pmid: 16177369
19. L. B. Lawson, E. B. Norton, J. D. Clements, Defending the mucosa: Adjuvant and carrier formulations for mucosal immunity. *Curr. Opin. Immunol.* **23**, 414–420 (2011). doi: 10.1016/j.coi.2011.03.009; pmid: 21511452
20. R. Belland, D. M. Ojcius, G. I. Byrne, Chlamydia. *Nat. Rev. Microbiol.* **2**, 530–531 (2004). doi: 10.1038/nrmicro931; pmid: 15248311
21. C. L. Satterwhite *et al*., Sexually transmitted infections among US women and men: Prevalence and incidence estimates, 2008. *Sex. Transm. Dis.* **40**, 187–193 (2013). doi: 10.1097/OLQ.0b013e318286bb53; pmid: 23403598
22. I. J. Bakken, *Chlamydia* trachomatis and ectopic pregnancy: Recent epidemiological findings. *Curr. Opin. Infect. Dis.* **21**, 77–82 (2008). doi: 10.1097/QCO.0b013e3282f3d972; pmid: 18192790
23. V. H. Hu, M. J. Holland, M. J. Burton, Trachoma: Protective and pathogenic ocular immune responses to *Chlamydia trachomatis*. *PLOS Negl. Trop. Dis.* **7**, e2020 (2013). doi: 10.1371/journal.pntd.0002020; pmid: 23457650
24. D. C. Mabey, V. Hu, R. L. Bailey, M. J. Burton, M. J. Holland, Towards a safe and effective chlamydial vaccine: Lessons from the eye. *Vaccine* **32**, 1572–1578 (2014). doi: 10.1016/j.vaccine.2013.10.016; pmid: 24606636
25. J. T. Grayston, R. L. Woolridge, S. Wang, Trachoma vaccine studies on Taiwan. *Ann. N.Y. Acad. Sci.* **98**, 352–367 (1962). doi: 10.1111/j.1749-6632.1962.tb30558.x; pmid: 13901337
26. R. L. Woolridge *et al*., Field trial of a monovalent and of a bivalent mineral oil adjuvant trachoma vaccine in Taiwan school children. *Am. J. Ophthalmol.* **63** (suppl.), 1645–1650 (1967). doi: 10.1016/0002-9394(67)94158-X; pmid: 6067317
27. R. L. Nichols, S. D. Bell Jr., N. A. Haddad, A. A. Bobb, Studies on trachoma. VI. Microbiological observations in a field trial in Saudi Arabia of bivalent rachoma vaccine at three dosage levels. *Am. J. Trop. Med. Hyg.* **18**, 723–730 (1969). pmid: 4897605
28. R. L. Nichols, S. D. Bell Jr., E. S. Murray, N. A. Haddad, A. A. Bobb, Studies on trachoma. V. Clinical observations in a field trial of bivalent trachoma vaccine at three dosage levels in Saudi Arabia. *Am. J. Trop. Med. Hyg.* **15**, 639–647 (1966). pmid: 5941182
29. S. Sowa, J. Sowa, L. H. Collier, W. A. Blyth, Trachoma vaccine field trials in The Gambia. *J. Hyg.* **67**, 699–717 (1969). doi: 10.1017/S0022172400042157; pmid: 5261212
30. J. Schachter, Overview of *Chlamydia trachomatis* infection and the requirements for a vaccine. *Rev. Infect. Dis.* **7**, 713–716 (1985). pmid: 3840910
31. D. C. Gondek, A. J. Olive, G. Stary, M. N. Starnbach, $CD4^+$ T cells are necessary and sufficient to confer protection against *Chlamydia trachomatis* infection in the murine upper genital tract. *J. Immunol.* **189**, 2441–2449 (2012). doi: 10.4049/jimmunol.1103032; pmid: 22855710
32. A. F. Radovic-Moreno *et al*., Surface charge-switching polymeric nanoparticles for bacterial cell wall-targeted delivery of antibiotics. *ACS Nano* **6**, 4279–4287 (2012). doi: 10.1021/nn3008383; pmid: 22471841
33. P. O. Ilyinskii *et al*., Adjuvant-carrying synthetic vaccine particles augment the immune response to encapsulated antigen and exhibit strong local immune activation without inducing systemic cytokine release. *Vaccine* **32**, 2882–2895 (2014). doi: 10.1016/j.vaccine.2014.02.027; pmid: 24593999
34. B. E. Batteiger, F. Xu, R. E. Johnson, M. L. Rekart, Protective immunity to *Chlamydia trachomatis* genital infection: Evidence from human studies. *J. Infect. Dis.* **201** (suppl. 2), S178–S189 (2010). doi: 10.1086/652400; pmid: 20524235
35. W. M. Geisler, S. Y. Lensing, C. G. Press, E. W. Hook 3rd, Spontaneous resolution of genital *Chlamydia trachomatis* infection in women and protection from reinfection. *J. Infect. Dis.* **207**, 1850–1856 (2013). doi: 10.1093/infdis/jit094; pmid: 23470847
36. R. C. Brunham, Immunity to *Chlamydia trachomatis*. *J. Infect. Dis.* **207**, 1796–1797 (2013). doi: 10.1093/infdis/jit095; pmid: 23470849
37. R. C. Brunham, J. Rey-Ladino, Immunology of *Chlamydia* infection: Implications for a *Chlamydia trachomatis* vaccine. *Nat. Rev. Immunol.* **5**, 149–161 (2005). doi: 10.1038/nri1551; pmid: 15688042
38. C. M. Farris, R. P. Morrison, Vaccination against *Chlamydia* genital infection utilizing the murine C. muridarum model. *Infect. Immun.* **79**, 986–996 (2011). doi: 10.1128/IAI.00881-10; pmid: 21078844
39. R. A. Hawkins, R. G. Rank, K. A. Kelly, Expression of mucosal homing receptor α4β7 is associated with enhanced migration to the *Chlamydia*-infected murine genital mucosa in vivo. *Infect. Immun.* **68**, 5587–5594 (2000). doi: 10.1128/IAI.68.10.5587-5594.2000; pmid: 10992458
40. N. R. Roan, T. M. Gierahn, D. E. Higgins, M. N. Starnbach, Monitoring the T cell response to genital tract infection. *Proc. Natl. Acad. Sci. U.S.A.* **103**, 12069–12074 (2006). doi: 10.1073/pnas.0603866103; pmid: 16880389
41. A. J. Olive, D. C. Gondek, M. N. Starnbach, CXCR3 and CCR5 are both required for T cell-mediated protection against *C. trachomatis* infection in the murine genital mucosa. *Mucosal Immunol.* **4**, 208–216 (2011). doi: 10.1038/mi.2010.58; pmid: 20844481
42. S. G. Morrison, R. P. Morrison, A predominant role for antibody in acquired immunity to chlamydial genital tract reinfection. *J. Immunol.* **175**, 7536–7542 (2005). doi: 10.4049/jimmunol.175.11.7536; pmid: 16301662
43. L. X. Li, S. J. McSorley, B cells enhance antigen-specific CD4 T cell priming and prevent bacteria dissemination following

Chlamydia muridarum genital tract infection. *PLOS Pathog.* **9**, e1003707 (2013). doi: 10.1371/journal.ppat.1003707; pmid: 24204262
44. R. C. Brunham, C. C. Kuo, L. Cles, K. K. Holmes, Correlation of host immune response with quantitative recovery of *Chlamydia trachomatis* from the human endocervix. *Infect. Immun.* **39**, 1491–1494 (1983). pmid: 6840846
45. T. Moore *et al*., Fc receptor-mediated antibody regulation of T cell immunity against intracellular pathogens. *J. Infect. Dis.* **188**, 617–624 (2003). pmid: 12898452
46. C. M. Farris, S. G. Morrison, R. P. Morrison, CD4$^+$ T cells and antibody are required for optimal major outer membrane protein vaccine-induced immunity to *Chlamydia muridarum* genital infection. *Infect. Immun.* **78**, 4374–4383 (2010). doi: 10.1128/IAI.00622-10; pmid: 20660610
47. D. F. Tifrea, P. Ralli-Jain, S. Pal, L. M. de la Maza, Vaccination with the recombinant major outer membrane protein elicits antibodies to the constant domains and induces cross-serovar protection against intranasal challenge with *Chlamydia trachomatis*. *Infect. Immun.* **81**, 1741–1750 (2013). doi: 10.1128/IAI.00734-12; pmid: 23478318
48. L. Madsen *et al*., Mice lacking all conventional MHC class II genes. *Proc. Natl. Acad. Sci. U.S.A.* **96**, 10338–10343 (1999). doi: 10.1073/pnas.96.18.10338; pmid: 10468609
49. C. L. Scott, A. M. Aumeunier, A. M. Mowat, Intestinal CD103$^+$ dendritic cells: Master regulators of tolerance? *Trends Immunol.* **32**, 412–419 (2011). doi: 10.1016/j.it.2011.06.003; pmid: 21816673
50. E. Mazzini, L. Massimiliano, G. Penna, M. Rescigno, Oral tolerance can be established via gap junction transfer of fed antigens from CX3CR1□ macrophages to CD103□ dendritic cells. *Immunity* **40**, 248–261 (2014). doi: 10.1016/j.immuni.2013.12.012; pmid: 24462723
51. J. R. McDole *et al*., Goblet cells deliver luminal antigen to CD103$^+$ dendritic cells in the small intestine. *Nature* **483**, 345–349 (2012). doi: 10.1038/nature10863; pmid: 22422267
52. G. Matteoli *et al*., Gut CD103$^+$ dendritic cells express indoleamine 2,3-dioxygenase which influences T regulatory/T effector cell balance and oral tolerance induction. *Gut* **59**, 595–604 (2010). doi: 10.1136/gut.2009.185108; pmid: 20427394
53. U. H. von Andrian, C. R. Mackay, T-cell function and migration. Two sides of the same coin. *N. Engl. J. Med.* **343**, 1020–1034 (2000). doi: 10.1056/NEJM200010053431407; pmid: 11018170
54. S. J. Davila, A. J. Olive, M. N. Starnbach, Integrin α4β1 is necessary for CD4$^+$ T cell-mediated protection against genital *Chlamydia trachomatis* infection. *J. Immunol.* **192**, 4284–4293 (2014). doi: 10.4049/jimmunol.1303238; pmid: 24659687
55. D. E. Wright, A. J. Wagers, A. P. Gulati, F. L. Johnson, I. L. Weissman, Physiological migration of hematopoietic stem and progenitor cells. *Science* **294**, 1933–1936 (2001). doi: 10.1126/science.1064081; pmid: 11729320
56. T. L. Denning, G. Kim, M. Kronenberg, Cutting edge: CD4$^+$CD25$^+$ regulatory T cells impaired for intestinal homing can prevent colitis. *J. Immunol.* **174**, 7487–7491 (2005). doi: 10.4049/jimmunol.174.12.7487; pmid: 15944246
57. D. M. Brainard *et al*., Induction of robust cellular and humoral virus-specific adaptive immune responses in human immunodeficiency virus-infected humanized BLT mice. *J. Virol.* **83**, 7305–7321 (2009). doi: 10.1128/JVI.02207-08; pmid: 19420076
58. A. K. Wege, M. W. Melkus, P. W. Denton, J. D. Estes, J. V. Garcia, Functional and phenotypic characterization of the humanized BLT mouse model. *Curr. Top. Microbiol. Immunol.* **324**, 149–165 (2008). pmid: 18481459
59. F. Sallusto, D. Lenig, R. Förster, M. Lipp, A. Lanzavecchia, Two subsets of memory T lymphocytes with distinct homing potentials and effector functions. *Nature* **401**, 708–712 (1999). doi: 10.1038/44385; pmid: 10537110
60. W. Weninger, M. A. Crowley, N. Manjunath, U. H. von Andrian, Migratory properties of naive, effector, and memory CD8$^+$ T cells. *J. Exp. Med.* **194**, 953–966 (2001). doi: 10.1084/jem.194.7.953; pmid: 11581317
61. D. Masopust *et al*., Dynamic T cell migration program provides resident memory within intestinal epithelium. *J. Exp. Med.* **207**, 553–564 (2010). doi: 10.1084/jem.20090858; pmid: 20156972
62. E. Bettelli *et al*., Reciprocal developmental pathways for the generation of pathogenic effector TH17 and regulatory T cells. *Nature* **441**, 235–238 (2006). doi: 10.1038/nature04753; pmid: 16648838
63. S. Jung *et al*., Analysis of fractalkine receptor CX(3)CR1 function by targeted deletion and green fluorescent protein reporter gene insertion. *Mol. Cell. Biol.* **20**, 4106–4114 (2000). doi: 10.1128/MCB.20.11.4106-4114.2000; pmid: 10805752
64. I. Bernstein-Hanley *et al*., Genetic analysis of susceptibility to *Chlamydia trachomatis* in mouse. *Genes Immun.* **7**, 122–129 (2006). doi: 10.1038/sj.gene.6364285; pmid: 16395389

ACKNOWLEDGMENTS

We thank E. Nigro for secretarial assistance, L. B. Jones for technical support, and the members of the von Andrian laboratory for discussion. The data presented in this manuscript are tabulated in the main paper and in the supplementary materials. Supported by NIH grants AI078897, AI069259, AI095261, and AI111595, a Harvard Innovation Award from Sanofi Pasteur, and the Ragon Institute of MGH, MIT and Harvard (U.H.v.A.); NIH grants U54-CA119349, U54-CA151884, and R37-EB000244 and the David Koch Prostate Cancer Foundation (R.L. and O.C.F.); NIH grant 1 R01-EB015419-01 (O.C.F.); NIH grant R00 CA160350 (J.S.); NIH grant T32 HL066987 (D.A.); NIH grant P30-AI060354 and the MGH Humanized Mouse Program by the Harvard University CFAR (A.M.T.); and NIH grant R01 AI062827, NIH grant R01 AI39558, and the Epidemiology and Prevention Interdisciplinary Center for Sexually Transmitted Diseases (NIH grant U19 AI113187) (M.N.S.). G.S. is a Max Kade foundation postdoctoral research exchange grant recipient. A.F.R.-M. acknowledges support from the MIT Portugal Program and the National Science Foundation (NSF-GRFP). G.S., A.R.F.-M., P.A.B., M.N.S., R.L., O.C.F., and U.H.v.A. are inventors on a patent application entitled "Nanoparticle-Based Compositions" (U.S. Application number PCT2014/029000; International Publication No. WO2014/153087) filed by Harvard University together with MIT and Brigham and Women's Hospital (BWH) that relates to the use of cSAP for mucosal vaccination. A.R.F.-M., R.L., and O.C.F. are inventors on a patent application entitled "pH Sensitive Biodegradable Polymeric Particles for Drug Delivery" (U.S. Application no. PCT2011/0065807) filed by BWH together with MIT that relates to the engineering of charge-switching particles. O.C.F., R.L., and U.H.v.A. disclose financial interests in BIND Therapeutics, Selecta Biosciences, and Blend Therapeutics, three biotechnology companies developing nanocarrier technologies for medical applications. BIND, Selecta, and Blend did not support the research in this study. Selecta and Blend have obtained licenses to a portion of the intellectual property described in this study. O.C.F., R.L., and U.H.v.A. are scientific founders and members of the Scientific Advisory Board and O.C.F. and R.L. are directors of Selecta Biosciences. O.C.F., R.L. and U.H.v.A. are members of the Scientific Advisory Board and O.C.F. and R.L. are scientific founders and directors of Blend Therapeutics. The following reagents used in the paper are subject to MTA: NR-1 transgenic mice, cSAP, cSP, and SAP. All reasonable requests for collaboration involving materials used in the research will be fulfilled, provided that a written agreement is executed in advance between BWH, MIT, or Harvard Medical School and the requester (and his or her affiliated institution). Such inquiries or requests for additional data should be directed to the corresponding author.

SUPPLEMENTARY MATERIALS

www.sciencemag.org/content/348/6241/aaa8205/suppl/DC1
Figs. S1 to S10
31 January 2015; accepted 27 May 2015

10.1126/science.aaa8205

A mucosal vaccine against *Chlamydia trachomatis* generates two waves of protective memory T cells

Georg Stary *et al.*

Science **348**, (2015);
DOI: 10.1126/science.aaa8205